Results in Chemistry 16 (2025) 102322

Contents lists available at ScienceDirect

Results in Chemistry

journal homepage: www.sciencedirect.com/journal/results-in-chemistry

Advancements in calcium ferrite-based photocatalysts: Insights into their synthesis and performance in degrading organic pollutants

Behram Shehzad [a], Muhammad Hamid [a], Aqsa Batool [a], Muhammad Umer Shafique [a], Ayoub Rashid [a], Nabisab Mujawar Mubarak [b,c], Omirserik Baigenzhenov [d], Andrei Ivanets [e], Mahesh Kumar Sah [f], Ahmad Hosseini-Bandegharaei [g,h,i,*]

[a] Department of Chemistry, Government College University, Lahore, 54000, Punjab, Pakistan
[b] Chemical and Energy Engineering, Faculty of Engineering, Universiti Teknologi Brunei, Bandar Seri Begawan BE1410, Brunei Darussalam
[c] Centre for Research Impact & Outcome, Chitkara University Institute of Engineering and Technology, Chitkara University, Rajpura 140401 Punjab, India
[d] Department of Metallurgical Engineering, Satbayev University, 22a Satbaev Str., Almaty, 050013, Kazakhstan
[e] Institute of General and Inorganic Chemistry of the National Academy of Sciences of Belarus, Minsk 220072, Belarus
[f] Department of Biotechnology, Dr. B. R. Ambedkar National Institute of Technology, Jalandhar, Punjab, 1440081, India
[g] Faculty of Chemistry, Semnan University, Semnan, Iran
[h] University Centre for Research & Development, Chandigarh University, Mohali, Punjab 140413, India
[i] Department of Sustainable Engineering, Saveetha School of Engineering, SIMATS, Chennai, Tamil Nadu 602105, India

ARTICLE INFO

Keywords:
Photocatalysis
Calcium ferrite
Degradation
Nanotechnology
Water treatment
Organic pollutants

ABSTRACT

Over the past two centuries, photocatalysis—the use of light to accelerate chemical reactions—has undergone substantial development. This multidisciplinary field, which is especially thriving with advances in nanotechnology, combines photochemistry, catalysis, and semiconductor physics. Calcium ferrite's low band gap and strong activity underneath sunlight make it a suitable for photocatalytic applications. The effectiveness of calcium ferrites and the related photocatalysts in organic pollution remediation, synthetic techniques, and their photocatalytic characteristics, including the processes governing their activity, are all covered in this paper. Numerous synthesis methods have been explained, including sol-gel, co-precipitation, and hydrothermal processes. The optical and structural characteristics have been examined using characterization methods like as UV–Vis spectroscopy and X-ray diffraction (XRD). The review demonstrates calcium ferrites' potential in environmental remediation technologies by highlighting how well it breaks down organic contaminants in water purification and, at the end, the challenges and future outlooks have been mentioned.

1. Introduction

Environmental pollution is increasing as time elapses due to escalating human population and fast industrialization. Water pollution is a class of environmental pollution that degrades the environment significantly and causes hazards to the living organisms found in the myriad ecosystems comprising the environmental strata. Water is contaminated by organic pollutants that originate from several industries, leachate percolation from garbage and solid wastes, household disposals and leachate leakage from landfills into groundwater reserves.

There are multiple methods (destructive and non-destructive) for the removal of traces of organic pollutants from water [1]. Non-destructive methods such as filtration, coagulation, electrocoagulation and flocculation remove the impurities without affecting the fundamental characteristics of water. Destructive methods such as biodegradation processes chemically and nearly completely transform the pollutant molecules. Ultraviolet (UV) and UV-related advanced oxidation processes like UV/hydrogen peroxide, UV/free chlorine and UV/per sulfate are noteworthy techniques that are used to remove of trace organic pollutants. However, some pollutants do not degrade under UV light. For the degradation of such pollutants, photolysis-based advanced oxidation processes are being explored [2]. These processes can be particularly useful in degrading organic pollutants [3]. Photocatalysts have a strong potential to degrade organic pollutants into less harmful species namely water and carbon dioxide [4]. Physicochemical attributes such as huge (specific) surface area, excellent morphology with adequate pore

* Corresponding author at: Faculty of Chemistry, Semnan University, Semnan, Iran
E-mail address: ahoseinib@yahoo.com (A. Hosseini-Bandegharaei).

https://doi.org/10.1016/j.rechem.2025.102322
Received 16 February 2025; Accepted 2 May 2025
Available online 16 May 2025
2211-7156/© 2025 The Authors. Published by Elsevier B.V. This is an open access article under the CC BY license (http://creativecommons.org/licenses/by/4.0/).

connectivity and porosities, shorter band gap, and good crystallinity are much sought after in photocatalysts that are to stand out in prime line for scale-up endeavors engendered in water remediation.

Photocatalysis has a relatively significant history over the last two centuries. Photocatalysis were first mentioned in literature in the early 1910s, following which work in this field started to wax at a global scale in various research groups. In the early research episodes, scientists in Europe found out that the uranyl ion [5,6] as well as the actinide ion showed excellent photochemical properties. Both are still used today in photochemical reactions. In the 1960s, Russian, Japanese and German research groups began investigating photocatalytic processes using materials such as ZnO and TiO_2 [7]. In the 1970s, the oil crisis spurred research in alternative energy types, leading to the pivotal work of Fujishima and Honda [7] on electrochemical water photolysis. Nozik [8] later demonstrated water splitting without external potential, and TiO_2 emerged as a prominent photoactive material [9,10]. The fascinating nature of photocatalysis is interdisciplinary and it is related to photochemistry, catalysis and semiconductor physics. Recently, photocatalysis has found vast applications in hydrogen (H_2) production, reduction of carbon dioxide, purification processes and nitrogen fixation [11,12]. Leaps in nanotechnology offer promising possibilities, despite concerns about the materials' toxicities and other factor that can influence their respective efficiency under different conditions. Currently, photocatalysis has become a green and ecofriendly technology base (without consumption of fossil fuels) to resolve several problems (questions) of this era [13].

The photocatalytic mechanism (Fig. 1) involves a catalyst undergoing (starting) a chemical reaction under the effect of sunlight, and proceeds by multiple steps. The first step involves the exposure of the photocatalyst to visible light (sunlight). Calcium ferrite, being a p-type semiconductor [14–16], plays a crucial role in photocatalysis, according to the positions of valence and conduction bands. The minimum position of the conduction band of calcium ferrite is usually found at a comparatively low potential, for instance, at about −0.6 V vs RHE, which allows it to effectively reduce organic pollutants by receiving electrons from the photocatalytic reaction. The opposite is where the valence band maximum appears in order to activate the degradation of water or organic compounds via release of holes that are paramount to degradation. Calcium ferrite, typically its band gap measures 1.9 eV, can accept visible light making it efficient enough for harnessing the sun energy into photocatalysis. By absorbing light, electrons form the valence band get excited and move upward towards the conduction band. This movement of electrons creates a positive charge (a hole) in the valence band and a negative charge (electron) in the conduction band. This electron-hole pair is the physical attribute that endows photocatalysis with its versatile range of applications [17]. The electron in the conduction band reacts with water's oxygen to form superoxide ion radical $^{\bullet}O_2^-$ and the h^+ (hole) reacts with OH group of water to form the hydroxyl moiety, $OH^{\bullet}$. The superoxide radical ion reacts with h^+ to form $OH^{\bullet}$ which undergoes further degradation [18,19]. The hydroxyl radical undergoes oxidation when converting harmful contaminant compounds to less harmful products such as water and carbon dioxide [20]. In modern terms, these chemical reactions fall under the category of Advanced Oxidation Processes [21–23].

The following equations relate the phenomena of photocatalysis as mentioned above [24];

$$\text{Photocatalyst} + h\gamma \rightarrow e^- + h^+ \quad (1)$$

$$H_2O + h^+ \rightarrow OH^{\bullet} + H^+ \quad (2)$$

$$H_2O + e^- \rightarrow {}^{\bullet}O_2^- \quad (3)$$

$${}^{\bullet}O_2^- + H^+ \rightarrow OH^{\bullet} \quad (4)$$

$$OH^{\bullet} + \text{Contaminant} \rightarrow H_2O + CO_2 \quad (5)$$

2. Significance of calcium ferrite in photocatalytic applications

Photocatalysis, an advanced oxidation, has received a relatively huge attention over a long period of time [11,25]. Selecting a good photocatalyst is crucial for efficient elimination of persistent pollutants. For many years, titanium dioxide (TiO_2) and zinc oxide (ZnO) have been favorite candidates due to their photocatalytic activity. However, both of these chemicals are hampered by high band gaps (3.2 eV and 2.37 eV, respectively) and UV light, which restricts their activity towards simulated sunlight, as shown in Table 1 [26,27]. To overcome this limitation, more recent photocatalysts such as bismuth-based compounds, silver-doped materials, and graphitic carbon nitride have been developed, showing higher efficiency under visible light. Despite such advancements, the effective recyclability and reusability of these materials

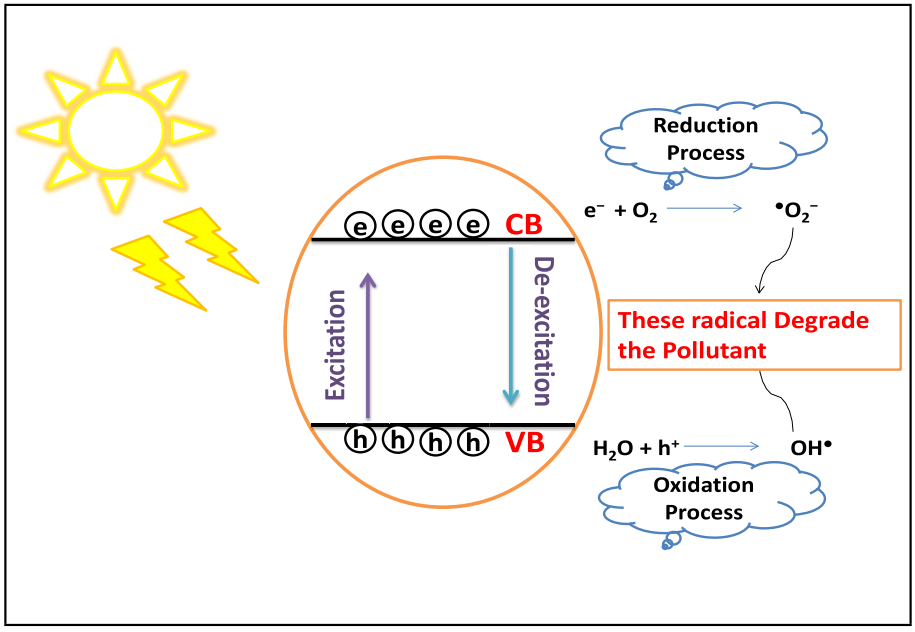


Fig. 1. Mechanism of photocatalysis.

Table 1
Comparative analysis of metal ferrites, TiO_2, ZnO as potential photocatalyst.

Characteristics	Metal Ferrites	ZnO	TiO_2
Light Absorption	Narrow band gap (1.5–2.3 eV) leads to absorption of visible light	Band gap nearly 3.7 eV leads to the absorption of Ultraviolet light	Band gap in range of (3.0–3.2 eV) efficiently activated under UV light
Stability and Reusability	Better stability and biocompatibility over multiple use	Good stability, and limited reusability due to corrosion in lengthened UV light	Excellent reusability, and stability over multiple times
Environmental Impact	Ecofriendly and non-toxic in nature	Potentially toxic for various marine animals	Potentially toxic for various marine animals
Synthesis Methods	Commonly synthesized by sol-gel, co-precipitation and etc.	Generally synthesized b chemical precipitation, hydrothermal, and also green synthesis methods	Can be synthesized via CVD, PVD, gas-phase, and solid phase method

present significant challenges, where further research is required on material properties and optimization [28–30].

To combat the intense difficulties with lack of efficiency in photocatalysis, magnetic photocatalysts have emerged as preferred options. Some magnetic photocatalysts are more efficient under visible light conditions, i.e., sun, and tend to have a narrower band gap, promoting greater photocatalytic efficiency. One of the strongest advantages with magnetic photocatalysts is their recyclability, allowing controlled exposure periods over test samples that can be optimized as a process variable [31,32].. Among the leading categories of magnetic photocatalysts, metal ferrites (MFe_2O_4) stand out due to their low band gap and ability to function effectively using sunlight [31,33,34].. Within the family of metal ferrites, such as nickel [35–37], manganese [38,39], cobalt [40–42], calcium [32,43], and zinc [36] types, calcium ferrite ($CaFe_2O_4$) has been of notable interest [32]. This is due to its extremely low toxicity, non-polluting nature, and high chemical stability compared to other transition metal ferrites [44,45].

Indeed, in the last few years, calcium ferrite ($CaFe_2O_4$) has emerged as a good magnetic photocatalyst due to its unique features. Its comparatively smaller band gap of approximately 1.9 eV allows it to absorb low-energy photons [46] (Table 2), predominantly from the visible light, which enhances the degradation of contaminants and promises a better future for environmental remediation. Additionally, the magnetic property of calcium ferrite facilitates easier recovery from reaction media, making it more convenient and efficient compared to traditional materials. The comparatively low toxicity and improved chemical stability of calcium ferrite compared to other transition metal ferrites are the additional reasons for drawing growing interest in photocatalytic applications. As a member of the broad family of magnetic photocatalysts, calcium ferrite possesses the advantage of being active under visible light and reusable, with exposure time under control as a process parameter.

Table 2
Comparison of different metal ferrites.

Characteristics	$CaFe_2O_4$	$CoFe_2O_4$	$ZnFe_2O_4$	$NiFe_2O_4$	$MgFe_2O_4$
Band Gap (eV)	1.90 [59]	2.27 [60]	2.02 [61]	2.26 [62]	2.0 [63]
Specific Surface Area ($m^2\ g^{-1}$)	82	91	134	135	83

A recent example study that demonstrates this potential is when $CaFe_2O_4$, with a 7.1 wt% Fe loading, produced an 86.1 % removal efficiency for high 2-chlorophenol after 180 min of UV–visible light [47]. This $CaFe_2O_4$ photocatalyst could be effectively reused, with a relatively high removal efficiency of 70.5 % for 2-chlorophenol after the third cycle, with no regeneration (re-calcination or washing). In another study, a nanostructured semiconductor calcium ferrite altered with carbon quantum dots, synthesized by a simple hydrothermal method, produced a 90 % photocatalytic degradation of Congo red dye under visible light [48]. Beside photocatalytic applications, calcium ferrite also finds use in the steel making industry [49,50], in optical memory devices design [51], high temperature sensors [52,53] and magneto plumbite structure [51].

Calcium-doped ferrite with a band gap of 1.9 eV exhibits superior catalytic activity in visible-light photochemical reactions compared to cobalt-doped and nickel-doped ferrites with greater band gaps of 2.27 eV and 2.26 eV, respectively. Its superior performance is primarily attributed to the smaller band gap of calcium-doped ferrite, which allows it to absorb more visible light and generate more charge carriers that are necessary to initiate photocatalytic reactions. The organic pollutants are broken down by the generation of reactive species such as hydroxyl radicals and superoxides with the assistance of photogenerated holes and electrons. Its low toxicity and saturation magnetization, brought about by the reason that calcium is an alkaline earth metal embedded in the ferrite lattice, help it to be suitable for environmental applications, as compared with potentially harmful transition metals [54]. Additionally, calcium ferrites are structurally stable in the form of a crystalline structure, which declines the likelihood of metal ion release and subsequent toxicity. Beside this, calcium ferrite also has low equilibrium time, as compared to other metal ferrite [43]. However, while calcium ferrite has potential photocatalytic activity due to its narrow band gap, synthesis methods may impact its overall performance [55]. Techniques like electrospinning might yield materials with higher surface areas [56], potentially exceeding materials produced via conventional ceramic methods. However, sophisticated synthesis methods can circumvent homogeneity issues associated with traditional methods, thereby improving the photocatalytic activity of calcium ferrite [56–58].

3. Common synthesis methods of calcium ferrite

3.1. Co – Precipitation

3.1.1. Description of the method

The co-precipitation method (Fig. 2) is the one of the finest methods for fabricating nanocrystals because it provides the opportunity to control the size of crystals, and thus enable production of high as well as low size grains. Nanoparticles that are synthesized by this method have the following features: good Crystallinity, excellent textural properties, homogeneity, high yield and relatively broad size distribution [64]. This method is especially preferred for the synthesis of small sized particles [65–68]. For the synthesis of calcium ferrite, equal concentrations of nitrates of calcium and iron are dissolved in 150 mL of distilled water at room temperature (Fig. 2). For proper mixing, the solution is stirred and ethylene glycol is added as a surfactant to obtain a proper solution. After this, the pH of the solution is maintained up to 8 by addition of sodium hydroxide solution drop wise that also acts as a precipitating agent. Then, this solution is stirred on hot plate for an hour to produce particles of the best possible size. This solution is then centrifuged with ethanol as well as distilled water after the precipitate has been synthesized so as to recuperate the precipitate at the end of centrifuge tube. After washing,

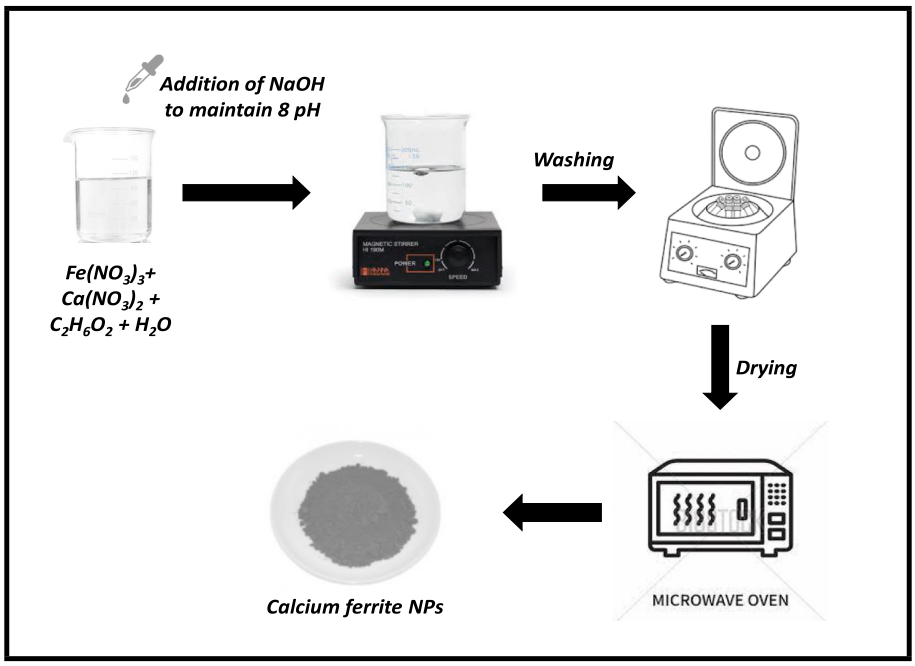


Fig. 2. Flow chart diagram of Co-Precipitation Process.

precipitate is dried in an oven at 80–90 °C for 6 h to obtain the calcium ferrite nanoparticles [68–70].

3.1.2. Key parameters influencing co-precipitation synthesis

Temperature, concentration of salt precursor and pH are the main parameters that influence the synthesis of calcium ferrite. The temperature of the system has significant effects on structure and size of synthesized NPs. As the temperature of the system is raised, it will facilitate synthesis of small sized nanoparticles with more uniformity and crystallinity. This is because of maximum temperature that provide sufficient energy to atoms to get more stable, crystal sized structure. Conversely, low temperature system provides large sized particles with low crystallinity due to insufficient energy for atoms to get arrange themselves in well-defined structure. Recent studies have proven that optimal temperature range provide us tunable size and shape which ultimately affects the catalytic and magnetic properties of synthesized material [71,72]. The concentration of calcium ferrite has direct impact on the particle size of NPs. Higher concentration of precursor means more metal ions in solution which enhance the nucleation rate ultimately leads to the large clusters. Optimized concentration must be required to get desired size of synthesized NPs [73]. The pH of system is one of the crucial parameter that influence the properties of calcium ferrite. System with high pH value enhance the particle size by lowering electrostatic repulsion between particle and forming large cluster. On the other hand, system with low pH help to produce small size particle [74].

3.2. Sol-gel method

3.2.1. Overview of the sol-gel process

The sol-gel method is another method for producing calcium ferrite nanoparticles. It has multiple pros over other methods which include being a relatively cheap method (less expenditures), being simpler, it confers more uniformity to the nanoparticles, and there is monodispersity and homogeneity in the microstructures [43,44,75]. The major reason for preferring the sol-gel method over others is its minimum energy utilizations, its safety records, and its overall easy and fastness [54,68]. During the sol-gel method, a salt precursor undergoes hydrolysis and a condensation process results in the formation of a 3D network of ions [76,77]. Following hydrolysis, M-OH group is formed. As these groups combine or condense with each other, they yield hard to break and irreversible M-O-M bridges [78].

In the synthesis of calcium ferrite by the sol-gel method (Fig. 3), equal concentrations of nitrates of iron and calcium are added in 100 mL of distilled water. A chelating agent (2 mol L^{-1} citric acid) is used to stabilize the structure within the aqueous solution thus produced. Then, the solution is stirred for a period of time at 80 °C. After addition of ethylene glycol to this mixture, it turns into a gel-like brownish material. The gel is dried in an oven for 8–10 h and it is then calcined at 550 °C for two hours to produce a powdered form of calcium ferrite particles [43] [68] [54,79].

3.2.2. Factors affecting the sol-gel synthesis of calcium ferrite

The properties of the gel depend upon different factors including the physicochemical characteristics of the solvent, the precursor's concentration, pH of solution, calcination temperature and degree of agitation. The choice of suitable solvent is the foremost in administering the solubility of synthesized material. Polarity and dissolution attributes considerably affects the structural properties of NPs. The growth of nanoparticles directly relate with nucleation rate which mainly depend upon concentration of precursor. High concentration of precursor leads to strong aggregation of metal ions, which yield better size of NPs. On the other hand, low concentration of precursor lead to high surface area with smaller size NPs. The concentration of the salt precursor affects the properties of the nanoparticles because different metal salts possess different magnetic properties that individually can lead to a variety of magnetic nanoparticles [80]. Chemical behavior of synthesized NP generally depend upon the pH of solution. The pH of solution influence the dissolution properties of salt, stability of Intermediate product, and finishing product in solution. A moderate pH guarantees the excellent crystal of synthesized system. Temperature at which gel is calcined play a crucial role in determining the magnetic, size, and crystallinity of synthesized NPs. High temperature heating leads to grain growth, which eventually counterfeit the magnetic properties of material. Hence, optimal calcined temperature is pivotal to get NPs with perfect size, crystallinity and etc. The uniformity of synthesized material primarily depend upon rate of agitation. The rate of agitation has impact on nucleation rate by evenly allocating the precursor ion within solution.

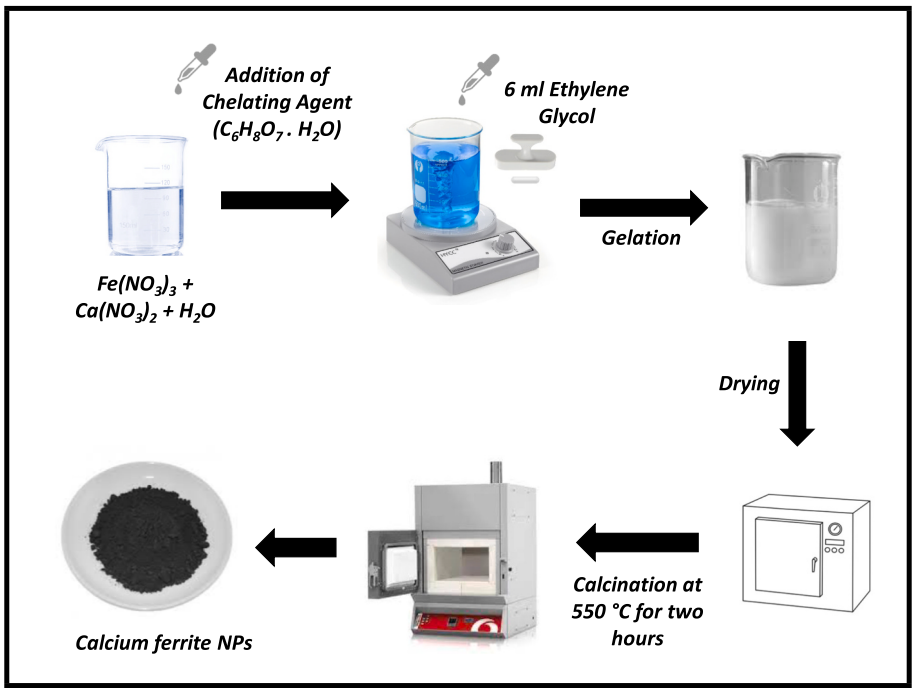


Fig. 3. Flow chart diagram of sol-gel method for preparation of calcium ferrite-based photocatalysts.

On the other hand, excessive or low agitation cause the formation of non-homogenize NPs [67]. Thus, all these factors act together, or in an order depicted in Fig. 3, to determine the specific synthesis of the magnetic calcium ferrite nanoparticles.

3.3. Hydrothermal synthesis

3.3.1. Explanation of the hydrothermal method

In relation to the synthesis methods of metal ferrites, the hydrothermal method has a pronounced significance among them all because of its relative cost effectiveness, convenience and simplicity and for the excellent morphology it confers to the ferrite nanoparticles [81–83]. It also endows the nanoparticles with high solubility, crystallization and diffusion properties and allows the analyst to have tune phase properties and control size transformation [84–86]. For the synthesis of calcium ferrite nanoparticles, nitrates of calcium, aluminum and iron are mixed in distilled water in equal stoichiometric concentrations and mixed properly (Fig. 4). Sodium hydroxide is then added in this solution as a starter/precursor. This solution's pH is maintained at about 9 to maintain a milieu whereby a good size is reached by the nanoparticles

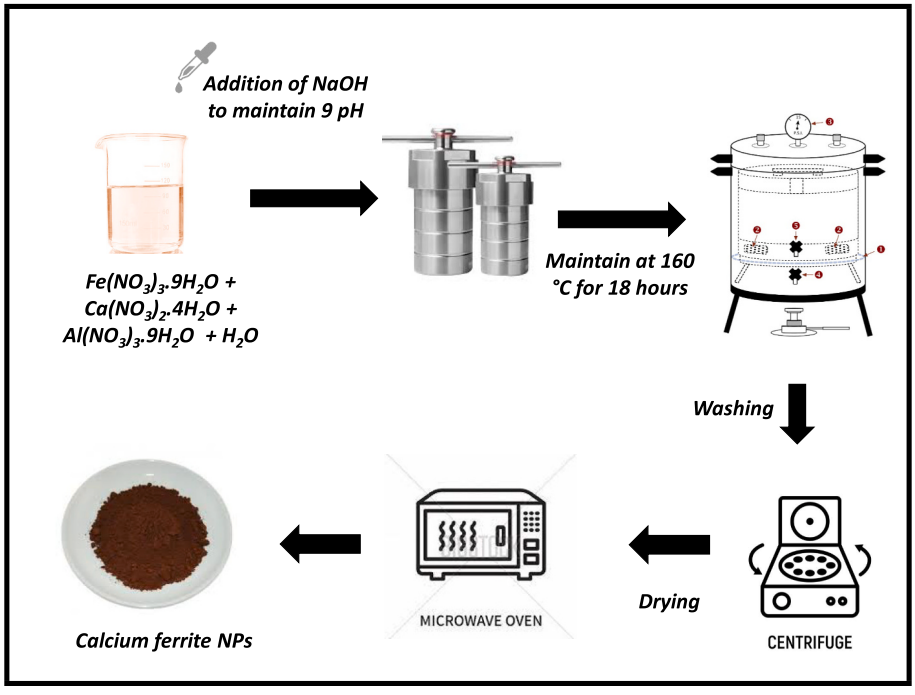


Fig. 4. Flow sheet diagram of hydrothermal synthesis of calcium ferrite-based photocatalysts.

(nucleation) [87] and is also stirred at 150 °C for nine hours. After this step, the solution is placed in a Teflon-lined stainless autoclave and kept at 160 °C for about 9–18 h [81,83]. At this high temperature, the reaction proceeds to form calcium ferrite nanoparticles. These nanoparticles are then cooled down and washed with distilled water and ethanol. After washing, the calcium ferrite nanoparticles are dried in an oven to recuperate its powder.

3.3.2. Variations and advances in hydrothermal synthesis

The pH of the solution, the concentrations of the protagonist species, the temperature at which the reaction steps proceed (annealing temperature) and the type of capping agent used are all important parametric factors that collectively influence the synthesis and final quality of the calcium ferrite nanoparticles [88] [89–91]. Constructive enhancements in the hydrothermal synthesis of calcium ferrite nanoparticles can eventually contribute in sustaining their use in photocatalytic processes. The use of microwaves for providing uniform heating to the mixture [92], the utilization of a surfactant that affects the growth rate and reduces agglomeration of nanoparticles [93], the replacement of batch reactor continuous flow systems [94] and in-situ monitoring [95] are all the different innovations that have reached the synthesis of calcium ferrite nanoparticles. For example, Ca-doped nickel ferrite ($Ni_{1-x}Ca_xFe_2O_4$) nanoparticles were prepared by a microwave combustion method. It was observed that the photocatalyst's efficiency improved with calcium doping up to a specific Ca content. Moreover, the photocatalytic degradation efficiency for one specific Ca-doped nickel ferrite (namely $Ni_{0.6}Ca_{0.4}Fe_2O_4$) for rhodamine B reached 99.69 % (Fig. 5), this performance being ascribed to the active parting and limited photo e^-/h^+-hole pair recombination [96]. In another study, calcium titanate ($CaTiO_3$) and calcium ferrite ($CaFe_2O_4$) nanostructures have been synthesized using a microwave assisted co-precipitation technique [97]. Results clearly demonstrated that both nanomaterial possessed photocatalytic properties. However, the $CaFe_2O_4/CaTiO_3$ composite had higher photocatalytic activity because of the coupling of two semiconductors. This coupling phenomenon could be put to service for a more effective charge separation and raising the lifetime in the charge carriers [97].

4. Characterization techniques

4.1. X-ray diffraction (XRD)

X-ray diffraction is a characterization technique that is used to analyze the crystallinity of nanoparticles. The crystallinity of NPs has crucial impact on efficiency of photocatalysis. Different size of NPs approaches active sites of organic pollutants differently which define the performance of the photocatalyst. XRD provides useful information about the phase composition, crystallographic properties and crystal structure of metal ferrites. For example, calcium ferrite showed same peaks (Table 4) as mentioned in the Joint Committee on Powder Diffraction Standards by [32,99]. The values of the unit cell parameters of calcium ferrite that have been revealed by XRD are given in Table 3.

4.2. Scanning electron microscopy (SEM) and transmission electron microscopy (TEM)

SEM and TEM are modern characterization techniques that help obtain data on the morphology, constitutions of synthesized powders at different length scales. Surface morphology is one of the key factor that relates to the absorption of light in photocatalytic reaction. An optimal structure provide maximum light penetration by well-organized charge transfer which eventually enhance the rate of degradation of Organic pollutants. The SEM of synthesized calcium ferrite nanoparticles shows that these nanoparticles are spherical. TEM helps us to inspect the internal components of photocatalyst which later may have impact on charge transfer in photocatalysis. The TEM of that spherical nanoparticle provides images of higher resolution and shows diameters ranging from 5 nm to 10 nm. Also, high surface energy and magnetic interaction between the nanocrystals cause them to agglomerate [100,101].

4.3. Fourier-transform infrared spectroscopy (FTIR)

The Fourier Transform Infrared Spectroscopy is a characterization technique that is used to detect functional group (bonds) in a given sample. Some functional groups may show strong affinity towards different organic contaminants that aided in the photodegradation of these contaminants. A number of peaks have showed up on the spectra including calcium oxide (Ca—O) and iron oxide (Fe—O) at 508 cm^{-1} and 442 cm^{-1} (Table 5). These bands are due to the stretching of these metal oxides. The stretching peak of the carbon-oxygen (C—O) bond shows up in the range of 1140–1170 cm^{-1} as mentioned in the literature [32,79,102].

Table 3
Calculated and Theoretical value of unit cell parameter of $CaFe_2O_4$ [32].

Unit cell Parameters	Theoretical (Å)	Calculated (Å)	Difference (Å)
A	9.228	9.218	0.0100
B	10.70	10.65	0.0500
C	3.018	3.031	0.0130

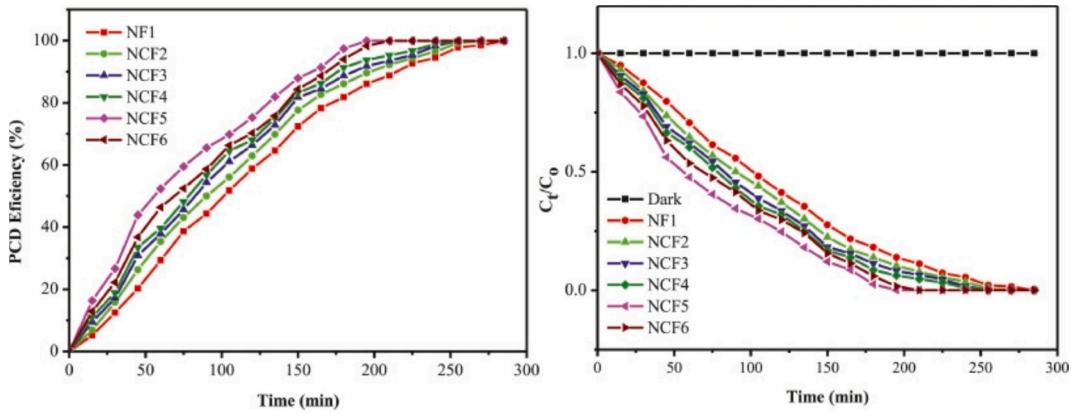


Fig. 5. Profiles for the (a) Photocatalytic degradation Efficiency (PCD), and (b) C_t/C_0 versus reaction time (min) of the Ca-doped nickel ferrite photocatalysts samples where NF1 stands for $NiFe_2O_4$, NCF2 is for $Ni_{0.9}Ca_{0.1}Fe_2O_4$, NCF3 denotes $Ni_{0.8}Ca_{0.2}Fe_2O_4$, NCF4 is for $Ni_{0.7}Ca_{0.3}Fe_2O_4$, NCF5 = $Ni_{0.6}Ca_{0.4}Fe_2O_4$, NCF6 designates $Ni_{0.5}Ca_{0.5}Fe_2O_4$, C_0 = initial rhodamine B concentration and C_t = concentration of rhodamine B in solution at time t. Reproduced with permission from [98].

Table 4
Data of XRD pattern of calcium ferrite nanoparticle [32].

Intensity (a.u.)	2 Theta (degree)
100	12.9
220	26.8
130	30.9
101	31.2
320	32.0
111	32.5
121	37.5
330	39.1
221	40.0
311	41.5
510	43.8
350	56.7
260	63.5
660	51.4
211	36.0

Table 5
Data of FTIR spectra of calcium ferrite nanoparticles.

$CaFe_2O_4$	IR Bands (cm^{-1})	Justification
	3786	O-H (stretching frequency)
	899	Fe-O-H (bending frequency)
	818	Fe-O-H (bending frequency)
	508	Ca-O (stretching frequency)
	442	Fe-O (bending frequency)

4.4. UV–vis spectroscopy

UV–Visible spectra provide data on the electronic absorption of a molecule that absorbs electromagnetic radiation of a specific wavelength of light. A strong absorption in visible region indicates the efficient degradation of dye under sunlight. Besides this, absorption data help us to find the band gap of that photocatalyst. Thus, the optical activity of a molecule under analysis can be elucidated to some extent using such analytical data. The UV–visible spectra of calcium ferrite show three different peaks at 262 nm, 364 nm and 463 nm. The peak at 262 nm lies in the ultraviolet part of the spectrum and is a strong one that represents calcium ferrite's maximum absorption (λ_{max}). The other two peaks are in the visible region [51]. The band gap of 1.9 eV for calcium ferrite is from the Tauc's equation [103,104].

5. Calcium ferrite Photocatalysts for dye degradation

Ferrites are excellent photocatalysts due to their low band gap [31,105]. Dyes are one of the major contributors to water pollution, and wield carcinogenic effects on aquatic life as well as on humans [106]. Dyes are organic compounds used to enhance the color property of materials such as textile, leather, paint, rubber printing [107]. Dyes are hugely used in industries because their respective color does not wane following the action of any attacking materials/moieties such as microbes, sugars, light and oxidizing agents [108]. The first ever dye was synthesized in 1856 by W.H. Perkin [109]. About 10 % of the dyes stuff used in industries is wiped out as a waste that cause pollution [110]. Chromophores and auxochromes are the major elements of dyes [111]. Chromophores are compounds or functional groups that provide color (also known as color bearing species) [112]. Auxochromes are groups that do not have color capacity but when attached with Chromophores, increase its coloring capacity (maximum absorption) [113]. Let alone calcium ferrite, its modification by doping of any metal or its composites with other photocatalyst yields better photocatalysts [47,64,114–117].

The **Evans blue dye** is a member of the azo dye (water soluble) class with a molecular weight of 960.83 g mol^{-1}. It was developed and first use by Herbert McLean Evans in 1914. Earlier, it was known as T-1824 and direct blue 53 [118,119]. The chemical structure of Evan blue dye is $C_{34}H_{24}N_6Na_4O_{14}S_4$ (Fig. 6(a)). Evans blue has major applications in medicine [120] including evaluation of blood volume and spotting of lymph node. Different concentrations of nanocomposites were synthesized and their respective degradation was studied under different conditions [121]. Table 6 shows the results of the degradation of Evans blue dye by calcium ferrite nanoparticles. Evans blue showed maximum adsorption upto 96 % at optimal condition of 40 mg/ 50 ml of catalyst dosage at pH of 2–6. It was seen that as the concentration of dye and temperature inversely relate with adsorption rate which resulted in lower degradation of dye. At the end, reusability of catalyst also be proven to be effective in degradation of Evans blue with slight low in efficiency.

Rhodamine B dye belongs to the class of xanthene dyes [122] with a molecular weight of 479.010 g mol^{-1}. As it dissolves in water, it is widely used as a dyeing agent for wool fabric. It maximum absorption (λ_{max}) is about 554 nm [96]. The chemical structure of Rhodamine B is $C_{18}H_{31}ClN_2O_3$ (Fig. 6 **(b)**). Besides its application in the textile industry, it is also used in medicine, plastic industry, as photosensitizer, water tracer and a biological strain in medicine [123–125].

The photodegradation of Rhodamine B and other textile reactive dyes were studied in [57] with Ag-free and Ag-coated calcium ferrite. In that study, firstly degradation was checked by use of silver coated and silver free calcium ferrite. It has been observed that silver coated photocatalyst show magnificent degradation with respect to silver free catalyst. As the concentration of photocatalyst increases from 2 mg/ml to 4 mg/ml, rate of degradation decreases. Beside the study of rhodamine Blue, other **Industrial reactive dyes** (red, blue and yellow) also been degraded by using silver coated photocatalyst. Degradation of these dyes goes upto 90 % for red, 65 % for yellow and 40 % for blue. Recently, an $Mg_{0.4}Zn_{0.1}Ca_{0.5}Fe_2O_4$ nano-ferrite gave very prominent photocatalytic degradation of Rhodamine B dye and antifungal activity

Table 6
comparative study of degradation rate of different dyes.

Dyes	Nanoparticle type	Concentration	Degradation rate	Photodegradation characteristic	Optical Band gap	References
Evans Blue	Calcium Ferrite	40 mg/50 ml (catalyst dosage), 3–25 ppm	Maximum efficiency: 96.11 % at 40 mg/ ml	Decrease adsorption at higher concentration of dyes and temperature (40–80 °C). slightly decrease in catalytic activity after reuse		[121]
Rhodamine B	Ag coated calcium ferrite	2 mg ml^{-2} (calcined)	Very fast degradation in first 5 min, then stabilization	For 3 mg mL^{-1}: pseudo first order kinetics. Degradation rate constant: o.o614 min^{-1}		[57]
Textile reactive dyes	Ag coated calcium ferrite	Red, yellow, Blue	Red: more than 90 % degradation. Yellow: 65 % after 2 h. Blue: 40 %	Ag–coated nanoparticle demonstrated efficient degradation, with silver incorporation improving charge separation		[57]
Methylene Blue	$Mg_{1-x}Ca_xFe_2O_4$	X = 0, 0.1, 0.2, 0.3	Decrease from 63 % (x=0) to 18 % (x = 0.1), increase to 38 % (x = 0.3)	Photodegadation of efficiency improves with increasing x. Best performance at x = 0.3	Band gap narrow from 1.97 eV (x = 0) to 1.87 eV (x = 0.2, 0.3)	[136]

Table 7
Selected features of studies reporting calcium ferrite-based photocatalytic degradation of organic compounds.

Photocatalyst	Synthesis method	Main properties	Organic compounds	Observations on photocatalytic degradation	Reference
Reduced graphene oxide/$CaFe_2O_4$/Ag_3PO_4 composite (mass ratio = 1:3:9)	Hydrothermal and ion-exchange deposition	Magnetically separable	Methyl orange, Methylene blue and 4-chlorophenol	Visible-light illumination-mediated photocatalytic dye degradation Photocatalyst endowed with high reusability and stability (first 5 cycles)	[137]
$CaFe_2O_4$ nanorods	Facile polymerizable complex method + Molten salt-assisted shape modification procedure	Grain boundaries are significantly less in structure	Methylene blue	Simulated solar irradiation for photocatalysis $CaFe_2O_4$ nanorods are significantly effective in degrading dye molecules (much enhanced kinetic constant of 0.013 min^{-1})	[138]
Pd-reduced graphene oxide/carbon nanotube/$CaFe_2O_4$	Facile method involving inclusion of carbon nanotubes into reduced graphene oxide	Magnetically separable photocatalyst	Methylene blue	Significantly higher photocatalytic degradation ability for methylene blue	[139]
Combined calcium ferrite and ZnO semiconductor with a solar active p–n heterojunction	Ball milling of ZnO in water that had been doped with $CaFe_2O_4$ (chemically, photocatalyst was synthesized by an in-situ hybridization process)	Narrower band gap of the heterojunction	Rhodamine B	Sunlight irradiation Significant portion of dye molecules mineralized during photoreduction	[140]
Hierarchical calcium ferrite core-shell hollow microspheres	Facile solvothermal method followed by heat treatment (Fig. 9(A))	Hollow structure conferred high surface area and considerably high visible-light absorption capability	1, 2-dichlorobenzene	After 8 h, degradation ratio = 82 % (Fig. 9(B)) Photodegradation under visible light irradiation (Fig. 9(C))	[141]
Calcium ferrite-N-doped graphene oxide nanocomposite	Ultrasonication-based method	Magnetic nanocomposite	*p*-nitrophenol and congo red	Visible light irradiation 88.2 % and 94.8 % photodegradation of congo red and *p*-nitrophenol, respectively	[142]
$Ca_{0.01}Fe_{2.99}O_4/CaTiO_3$ nanocomposite	Solvothermal method	Crystalline structure of magnetic composite Rectangular prismic structure of $CaTiO_3$ enhances photocatalytic dye degradation (more favorable band gap, enhanced surface characteristics, and better photo-induced charge separation efficiency)	Methylene blue	88 % photodegradation of dye observed under visible light illumination	[143]
g-C_3N_4/$CaFe_2O_4$ composite	Simple tactic polycondensation procedure (Fig. 10A)	Efficient absorption of visible light by composite Efficient charge carrier separation and transport through p-n heterojunction	Phenol and ciprofloxacin	Illumination provided by a Xenon lamp ($\lambda > 380$ nm, 500 W) $C_3N_4/CaFe_2O_4$ composite with an optimized $CaFe_2O_4$ content (i.e. with 50 mg calcium ferrite used in composite's synthesis) yielded phenol and ciprofloxacin photodegradation rates 2.1 and 2.3 times higher when compared to that obtained with virgin g-C_3N_4, respectively (Fig. 10B).	[144]
n-$CaTiO_3$/p-$CaFe_2O_4$	Hydrothermal method for $CaFe_2O_4$ preparation $CaTiO_3/CaFe_2O_4$ composites were synthesized following an in-situ growth procedure (Fig. 11A and Fig. 11B)	Heterojunction enabled the 'capture' of more visible light, suppressing of the recombination resulting from freshly produced oxygen vacancies and significant interfacial interaction	Tetracycline	p-n heterojunction inhibited recombination of visible light-induced electrons and holes, and this feature improved photocatalytic ability of the composite Light source: Osram 150 W Halogen lamp having two cut-off filters Best composite $CaTiO_3$@ $CaFe_2O_4$(0.50) photocatalyst yielded very good photodegradation (nearly 81 %) of tetracycline (Much higher than those obtained with virgin $CaFe_2O_4$ (45.1 %) and $CaTiO_3$ (nearly 21 %) (Fig. 11C)	[145]
$CaFe_2O_4$	Sol-gel method	BET surface area = 29.5 m^2 g^{-1} Effective charge separation of photoproduced e^-/h^+ pairs	Rose Bengal dye	Complete sunlight-induced photodegradation of dye within two hours Degradation kinetics was well	[146]

(*continued on next page*)

Table 7 (*continued*)

Photocatalyst	Synthesis method	Main properties	Organic compounds	Observations on photocatalytic degradation	Reference
				captured by the Langmuir-Hinshelwood equation	
Magnetic $ZnO/CaFe_2O_4$ nanocomposite	Hydrothermal method	Optimal cubic structure High abundance of reaction sites on composites *Z*-scheme heterojunction assists (e^--h^+) separation, thus enhancing redox reactions	T-2 toxin	Significantly high degree of mineralization reached (64 %, UV radiation for 180 min)	[147]

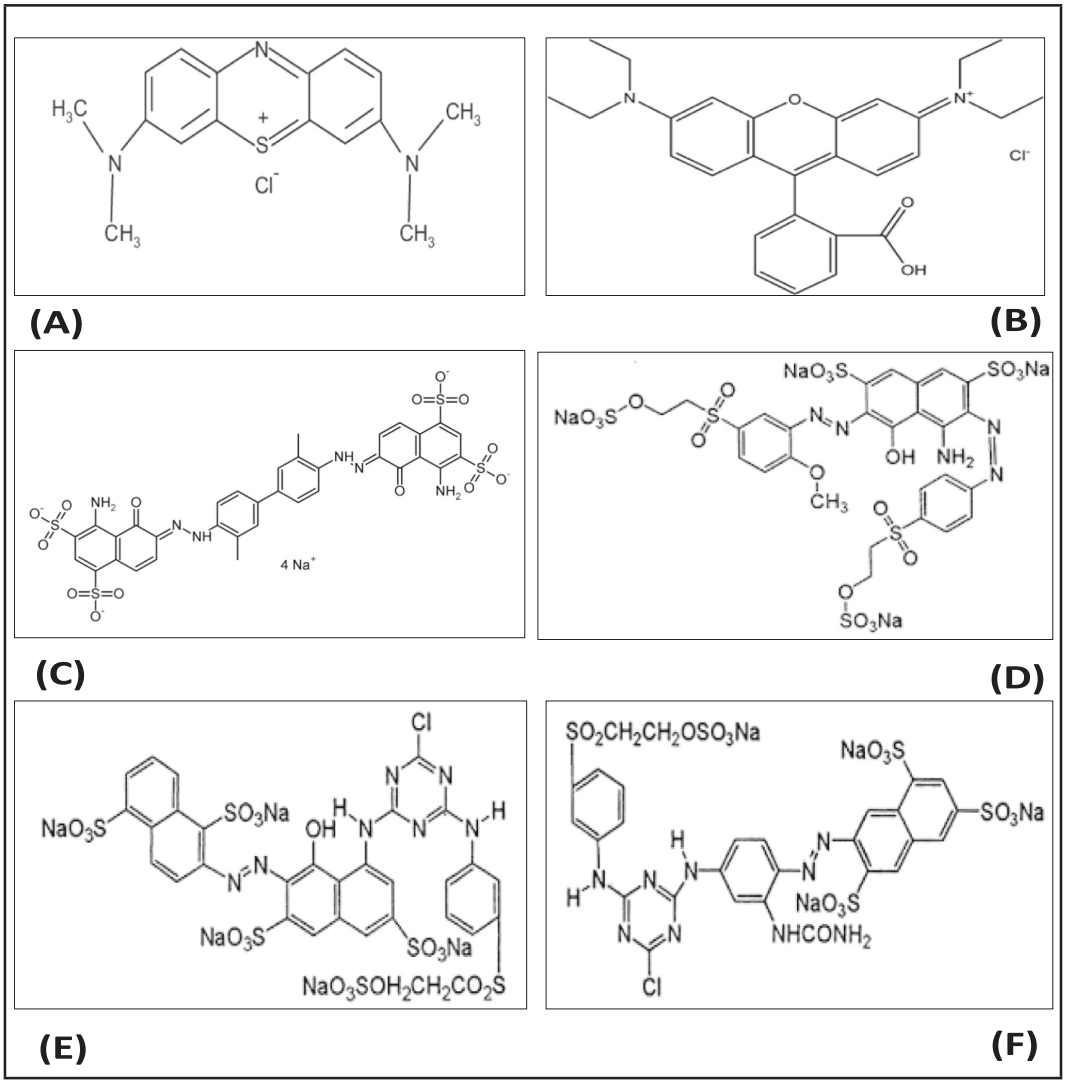


Fig. 6. Structure of different dyes degraded by calcium ferrite-based photocatalysts, including Evans blue, Rhodamine B and Methylene blue, Reactive Blue 250, Reactive Red 195, and Reactive Yellow 145. (For interpretation of the references to color in this figure legend, the reader is referred to the web version of this article.)

with no injurious impacts on the environment studied in the experimental tests [126].

Methylene blue is an cationic aromatic dye [127] that belongs to the phenothiazine family and has a molecular weight of 319.85 g mol^{-1} [128,129]. Methylene blue is one of the most used dyes, namely in the paper, cotton and textile (wool, silk) industries [130–132]. It is also used as a redox indicator [133]. It λ_{max} is about 663 nm [134]. Heinrich Caro was the first to synthesize methylene blue [135]. The chemical structure of methylene blue is $C_{16}H_{18}N_3ClS$ (Fig. 6 **(c)**). The degradation of methylene blue was studied in [136] with different compositions of $Mg_{1-x}Ca_xFe_2O_4$ nanoparticles. Different concentration of this nanoparticle proved that as the concentration increases band gap going to decrease which resulted in lowering photodegradation efficiency.

Sheet-on-sheet-like calcium ferrite (CF)-graphene nanoplatelets (GNPs) nanocomposites ($(CF)_{1-x}$ $(GNPs)_x$) produced very high photocatalytic activity via a 99.4 % efficiency for dye removal within 90 minutes [114]. The incorporation of the graphene nanoplatelets considerably augmented separation and movement of charge carriers.

The noteworthy electrochemical efficiency of these nanocomposites was attributed to the two-dimensional interfacial interactions that sustained a better transport of charges at the electrode-electrolyte interface. These interactions also allowed for effective charge transport routes and efficient electron/hole separation that caused fast dye degradation [114]. Interestingly, a $(CF)_{0.75}$ $(GNPs)_{0.25}$ nanocomposite exhibited the highest photocatalytic performance (Fig. 7). Interestingly, the photocatalytic performance decreased with higher GNPs content above 25 %. At a relatively low graphene ratio, an increase in photocatalytic activity can be observed with increasing graphene content. However, as the graphene ratio goes beyond a specific high value, photocatalytic activity starts to decline and this is associated with the more numerous GNPs hindering light from falling onto the photocatalyst's surface active site [114]. The observed photocatalytic activities (Fig. 7) resulted from the interplay of these phenomena. Cu-doped spinel calcium ferrite ($Ca_{1-x}Cu_xFe_2O_4$) nanoparticles were synthesized by a co-precipitation method [64]. The FTIR spectral bands of these nanoparticles observed at 579, 480 and 514 cm^{-1} established M − O vibration for the Ca—O, Fe—O and Cu—O bands that had caused spinel formation [64] Besides their notable magnetic behavior, the $Ca_{1-x}Cu_xFe_2O_4$ nanoparticles had band gaps of 1.8–2.5 eV, which indicated their semiconductor-like property (Fig. 8). Interestingly, a $Ca_{0.2}Cu_{0.8}Fe_2O_4$ nanocatalyst produced 96 % degradation of methylene blue dye in 180 min under UV-lamp irradiation [64]. This photocatalytic degradation's performance reported because of the small crystallite size and lower band gaps.

Table 7 summarizes the main aspects of other studies where the calcium ferrite-induced photocatalytic degradation of different organic molecules was recently studied. From these data sets, it becomes clear that calcium ferrite and its composites are receiving continual research attention. This is probably due to the versatility of calcium ferrite in being composited with different other materials by different synthetic routes, and thereafter degrading diverse types of organic molecules under varied experimental conditions. Indeed, so far, it is observed that the exceptional capabilities of calcium ferrite and its composites in photodegradation such organic compounds (Table 7) have been harvested at the laboratory scale. Such photodegradation performances are high promising and carry a great deal of scientific value in their own respective milieu. Notwithstanding these positive research advances, it remains a major research challenge and avenue for research and development to model and scale-up those calcium ferrite-dye and/or calcium ferrite-composite-dye laboratory systems which can carry adequate potential pilot-scale interest, first, and then be of more practical significance at an industrial scale.

The development of practical industrial-scale photocatalytic reactors is a major research and development challenge. This is ostensibly because there is limited data on the long-term optimized operation and maintenance requirements of such complex systems. The complexity of such systems will be a sum total of the effects from these design and operational parameters that will require continuous, real-time and on-line control: reactor size, design and configuration, temperature of aqueous environment, pH distribution across reactor, levels and distribution of dissolved oxygen within the reactor, concentration distributions of the photocatalyst across the reactor, concentration of target organic compounds, type and composition of real contaminated water, extent of influences of all of the most probable and most sensitive competing species and most probable competing sequestration mechanism such as biodegradation, biosorption and/or adsorption, type of illumination needed and sustenance of an as uniform and as optimal light penetration and light distribution with the different zones of the photocatalytic reactor, structural strength and chemical stability of photocatalyst, the specific type of interphase contacting between the aqueous media and the heterogeneous photocatalyst (e.g. stirred/slurry-type tank contacting, bubbling fluidized bed contacting or moving liquid-phase over inert media-supported photocatalysts).

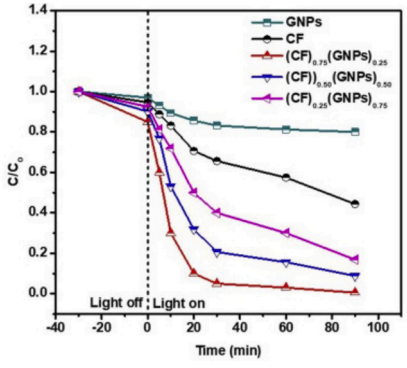


Fig. 7. Dye photodegradation processes by three $(CF)_{1-x}$ $(GNPs)_x$ nanocomposites. Reproduced with permission from [114].

6. Challenges and future perspective

While calcium ferrite-based photocatalysts show promise for environmental applications, challenges related to synthesis complexity, material purity, operational efficiency, and environmental stability must be addressed to enhance their practical utility in pollutant degradation processes. Continued research into optimizing synthesis methods and improving photocatalytic properties will be essential for advancing their application in real-world scenarios. As elaborated in this work, calcium ferrite-based photocatalysts are gaining attention for their potential in environmental remediation, particularly in the degradation of organic pollutants. However, several challenges arise in their synthesis and applications, which can be summarized as the follows.

1. The synthesis of calcium ferrite often requires complex and multi-step processes, which can involve high temperatures and specific conditions (e.g., hydrothermal treatment) that may not be easily scalable for industrial applications. To overcome the difficulty in synthesizing calcium ferrite at an industrial level, easier techniques such as the sol-gel or auto-combustion methods may be optimized. These techniques employ lower temperatures and fewer steps, which will be more suitable and cost-effective at an industrial level.
2. High-purity precursors are typically needed to achieve the desired photocatalytic properties. This requirement can increase costs and complicate the synthesis process. All one can do to address this challenge is exploiting cost-effective methods like sol-gel or the auto-combustion. These methods can produce nanoparticles with desired properties, thereby lessening the expenses by simplifying the synthesis process.
3. Achieving uniform particle sizes is crucial for optimal photocatalytic performance. Variations in particle size can lead to inconsistent catalytic activity and affect the efficiency of pollutant degradation. Synthesis pathways like solution combustion or sol-gel processes can be adjusted to achieve homogeneous particle sizes of calcium ferrite. Adding stabilizers and control of calcination temperatures can yield homogeneous sizes, resulting in improved photocatalytic activity and enhanced efficiency in pollutant degradation. Post-synthesis treatments can also be employed to reduce particle distribution.
4. While calcium ferrite exhibits some photocatalytic activity, its efficiency under visible light is often limited due to poor absorption properties. This restricts its effectiveness in practical applications where sunlight is the primary light source. Therefore, modification strategies should be adopted to dispel this shortcoming. Modification strategies can be employed, such as forming p–n heterojunctions with other materials like carbon nitride or loading metal cocatalysts like platinum. These modifications improve light absorption and charge separation, improving overall photocatalytic activity.

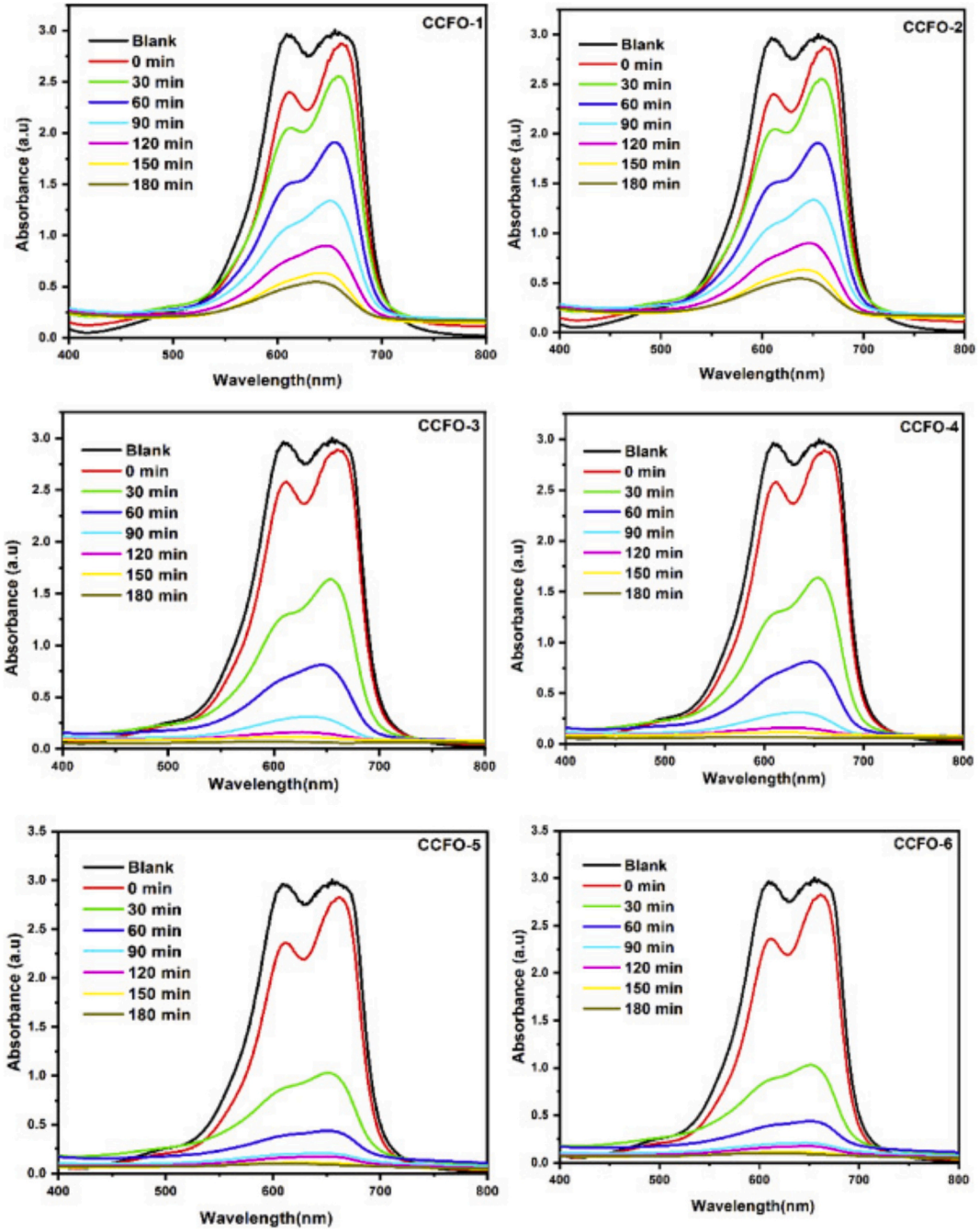


Fig. 8. Absorption spectra for the photocatalytic degradation performance of $Ca_{1-x}Cu_xFe_2O_4$ nanomaterial for methylene blue under UV lamp irradiation. CCFO-1 is when x = 0, CCFO-2 is for x = 0.2, CCFO-3 is for x = 0.4, CCFO-4 is when x = 0.6, CCFO-5 corresponds to an x = 0.8, CCFO-6 is when x = 1). Reproduced with permission from [64]. (For interpretation of the references to color in this figure legend, the reader is referred to the web version of this article.)

5. Fast recombination of electron-hole pairs generated during photocatalysis can significantly reduce the overall efficiency of calcium ferrite-based photocatalysts. Strategies such as doping with metals have been explored to mitigate this issue, but they add complexity to the synthesis process. However, strategies like forming p-n heterojunctions or metal Schottky junctions can enhance charge separation and transfer and improve photocatalytic efficiency without adding excessive synthesis complexity.
6. Photocorrosion and degradation of the photocatalyst under operational conditions can lead to reduced activity over time. Ensuring long-term stability while maintaining catalytic performance is a significant challenge. To address the challenge of obtaining long-term stability and catalytic activity of calcium ferrite photocatalysts, several strategies can be employed. Heterojunction formation and doping can improve photocatalytic activity and stability by promoting charge carrier separation and transfer processes. Surface modification processes such as coating with protective layers or coupling with other compounds such as carbon nitride can prevent photocorrosion and enhance durability. Furthermore, modulation of working conditions such as pH, temperature, and light intensity may minimize degradation. Recyclability and regeneration procedures need to be designed for reviving the catalyst activity during reuse. Finally, nanoscale engineering maximizes the interaction between the catalyst and reactants to result in enhanced efficiency and stability. Integrating these strategies could significantly enhance calcium ferrite photocatalysts' long-term activity.

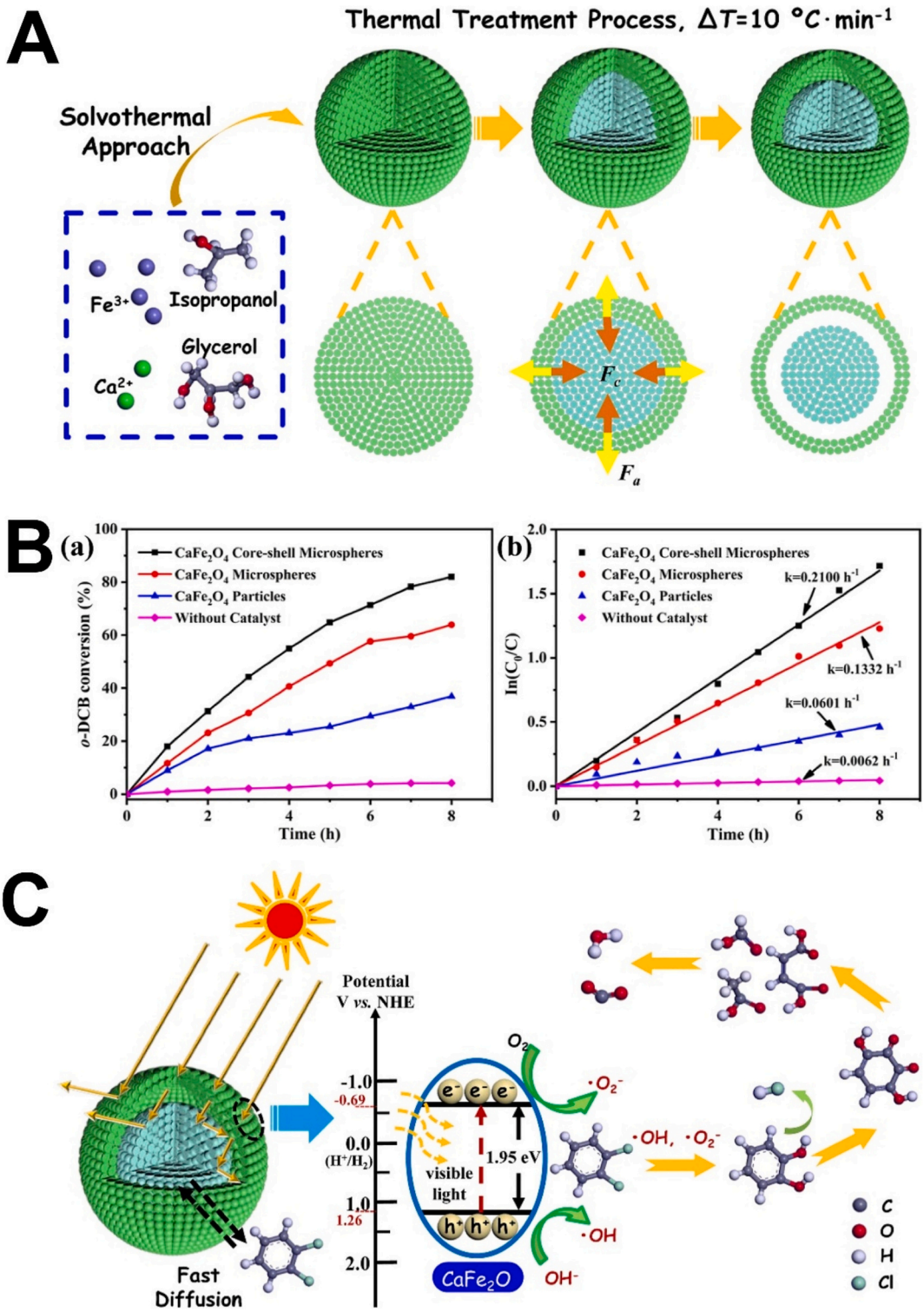


Fig. 9. **(A)** Proposed formation of calcium ferrite core-shell microspheres, **(B)(a)** Extents of photocatalytic degradation of *1, 2-dichlorobenzene* under the action of different catalysts and without catalyst, and **(B)(b)** the kinetic profiles for the corresponding photodegradation phenomena, and **(C)** proposed photodegradation mechanism of *1, 2-dichlorobenzene* over the calcium ferrite core-shell hollow microspheres reported in [141]. Images are reproduced with permission from [141].

7. The photocatalytic activity of calcium ferrite can be highly sensitive to pH levels, with optimal degradation occurring at specific pH values. Deviations from these conditions can lead to decreased efficiency due to the formation of unwanted by-products or catalyst deactivation. To get over this issue, it is important to maintain optimum conditions of pH. This can be achieved by pH control and adjustment during reaction. Additionally, wherever possible, pH buffers or stabilizers can be added to maintain the surroundings stable to prevent unwanted by-products along with catalyst deactivation. The appropriate modifications and designs can also stabilize the catalyst over a pH range.

Anyway, future of calcium ferrite-based materials as photocatalysts for degradation of organic pollutants looks promising due to increase in

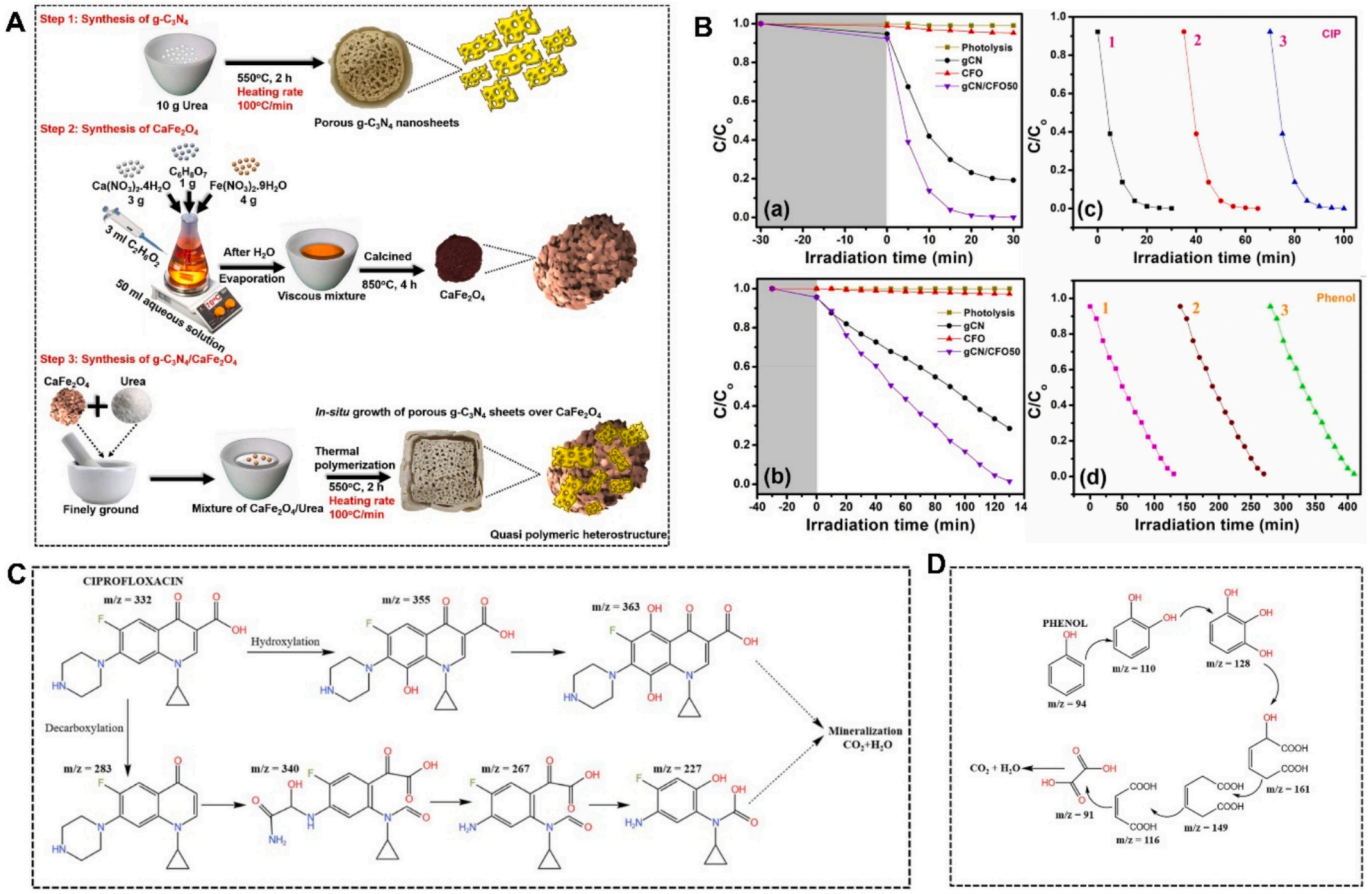
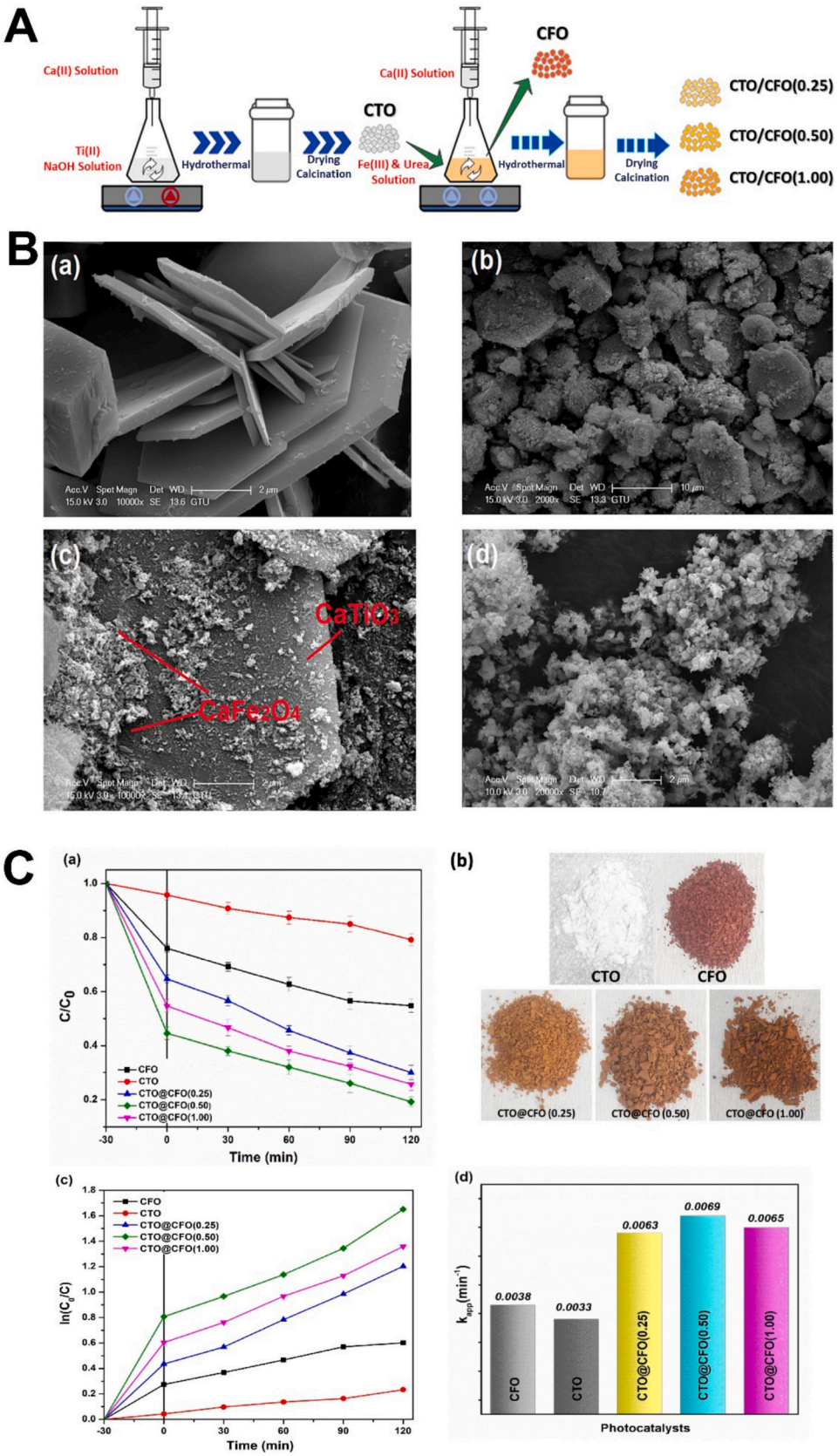


Fig. 10. **(A)** Steps in the in-situ tactic polycondensation method for preparing g-C_3N_4/calcium ferrite heterojunction, **(B)** photocatalytic degradation process of 10 ppm **(a)** ciprofloxacin (CIP) and **(b)** phenol under the effect of pure g-C_3N_4 (gCN), calcium ferrite (CFO), and gCN/CFO50 photocatalysts under visible light illumination (gCN/CFO50 denotes a composite material produced when 50 mg of as-synthesized calcium ferrite had been used in the production of the composite), and **(c)** and **(d)** stability of the optimal photocatalyst (i.e. gCN/CFO50) for 3 recurrent cycles of photodegradation of ciprofloxacin and phenol, respectively, **(C)** and **(D)** possible visible light-induced photodegradation mechanisms of ciprofloxacin and phenol under the action of the gCN/CFO50 composite, respectively, all reported in [144]. Images reproduced with permission from [144].

performance by doping with suitable metals that lower band gap and enhances the stability. Composites of calcium ferrite with graphitic carbon nitride or carbon nanotube had showed superb photocatalytic activity. In future, scientists can go for novel composites of calcium ferrite that future enhances the stability and efficiency of photocatalyst. Continued research into their synthesis, modification, and application will enhance their effectiveness and broaden their use in addressing global challenges such as pollution and energy sustainability. Future perspective and research direction of synthesis and use of calcium ferrite-based photocatalysts can include the following ones:

1. There are several ways to synthesize calcium ferrite, and each one affects the material's characteristics: Co-precipitation: This technique, which uses calcium and ferric salts as precursors, is preferred for its ease of use and affordability. It makes it possible to produce high-purity $CaFe_2O_4$ with regulated size and shape; Hydrothermal therapies: Recent research has demonstrated that $CaFe_2O_4$ may be produced while improving sustainability by using waste materials like eggshells. This method cuts manufacturing costs in addition to reducing waste; and Green synthesis: Because they are eco-friendly and may produce nanostructured particles with increased photocatalytic activity, biological material-based techniques are becoming more and more popular. In the future, scientists can concentrate on all of these tactics.
2. Since combining $CaFeO_4$ with materials like nitrogen-doped graphene oxide (NGO) has demonstrated notable increases in photocatalytic activity, a number of methodologies, such as nanocomposite production, can be further investigated to increase the photocatalytic efficiency of calcium ferrite. Doping and surface modification can optimize the band gap and enhance light absorption, making calcium ferrite effective under visible light irradiation; magnetic properties, as ferrites' inherent magnetic properties facilitate easy recovery and reuse after photocatalytic processes, which is crucial for practical applications in wastewater treatment; and the NGO improves charge carrier separation and light absorption, which results in better degradation rates of organic pollutants.
3. Photocatalysts based on calcium ferrite can still be effectively used in a number of fields like environmental remediation. Under UV–visible light, they have shown effective in breaking down contaminants like 2-chlorophenol and other organic colours. Research shows that $CaFe_2O_4$ may be utilized for solar water splitting and CO_2 reduction, which contributes to sustainable energy solutions. Studies also find excellent removal efficiency, demonstrating their promise in wastewater treatment applications.

Indeed, the future of calcium ferrite-based photocatalysts is bright, with a number of opportunities for more research, such as (i) adjusting synthesis parameters to improve material properties will be important, and investigating different precursors and methods may result in more effective catalysts; (ii) a better understanding of the photocatalytic mechanisms at work will aid in the design of more effective materials, and research should concentrate on clarifying how structural changes



(caption on next page)

Fig. 11. **(A)** Steps in the preparation of the $CaTiO_3/CaFe_2O_4$ (CTO@CFO) composites (note: CTO@CFO(0.50) denotes that the molar amount of CFO was 0.50 with respect to 1 mol of CTO), **(B)** SEM images depicting the morphologies and microstructures of the **(a)** $CaTiO_3$ (uniform nanostructured plates having a smooth surface with a fraction of these plates being grouped into a 'flower-like' microspherical crystalline structure), **(b)** and **(c)** CTO@CFO(0.50) (rod structured CFO dispersed and arranged over the nanoplates of parent $CaTiO_3$) and **(d)** bare $CaFe_2O_4$ (very small rod-shape structures clustered into spheres), and **(C)** (a) profiles depicting the photocatalytic degradation of tetracycline, **(b)** pictures of the different pristine materials and prepared composites analyzed, **(c)** kinetic plots for the corresponding photodegradation processes, and (d) their corresponding first-order reaction rate constants (k_{app} in min^{-1}), all reported in [145]. Images reproduced with permission from [145].

affect performance under various environmental conditions; (iii) creating scalable synthesis techniques that maintain performance while being economically viable will be crucial for industrial adoption, and it is also necessary to look into the long-term stability and reusability of these catalysts in real-world settings.

7. Conclusion

Calcium ferrite nanoparticles and their composites emerge as promising candidate in photo-catalytically-mediated reactions, offering a potential direction for a solution to various environmental challenges linked to water pollution. Their syntheses are possible by the co-precipitation, sol-gel, and hydrothermal methods. These methods enable the formulation and production of calcium ferrite nanoparticles with tailored properties. The spectroscopic characterization techniques provide insights into their structural and optical characteristics. The photocatalytic properties of calcium ferrite, including its mechanism and range of influencing factors, showcase its potential in addressing water pollution issues. The comparative analysis versus other photocatalysts reveals the strengths and weaknesses of calcium ferrite nanoparticles, highlighting its unique advantages, such as low toxicity and efficient utilization of sunlight. Furthermore, the diverse applications of calcium ferrite in water purification, particularly in the degradation of organic pollutants, underscore its significant potential for use in environmental remediation efforts. Overall, this review underscores the pivotal role of calcium ferrite and its various composites in advancing photocatalytic technologies for sustainable environmental management. However, major research and development feats have to be addressed before the scale-up of any feasible aqueous-phase laboratory-scale photocatalytic degradation system. Cost considerations, reasonable cost estimations and finally cost optimization will all be imperative at the different stages of such an engineering and technology undertaking.

CRediT authorship contribution statement

Behram Shehzad: Writing – original draft, Investigation, Formal analysis, Conceptualization. **Muhammad Hamid:** Writing – original draft, Investigation, Formal analysis, Conceptualization. **Aqsa Batool:** Writing – original draft, Investigation, Formal analysis, Conceptualization. **Muhammad Umer Shafique:** Software, Investigation, Formal analysis, Conceptualization. **Ayoub Rashid:** Writing – original draft, Investigation, Formal analysis, Conceptualization. **Nabisab Mujawar Mubarak:** Writing – original draft, Validation, Methodology. **Omirserik Baigenzhenov:** Writing – review & editing, Investigation, Conceptualization. **Andrei Ivanets:** Writing – review & editing, Writing – original draft, Validation, Investigation. **Mahesh Kumar Sah:** Writing – original draft. **Ahmad Hosseini-Bandegharaei:** Writing – review & editing, Writing – original draft, Supervision, Software, Project administration, Methodology, Investigation, Formal analysis, Conceptualization.

Declaration of competing interest

The authors declare that they have no known competing financial interests or personal relationships that could have appeared to influence the work reported in this paper.

Data availability

No data was used for the research described in the article.

References

[1] N. Malouchi, et al., The removal of per-and poly-Fluoroalkyl substances from water: a review on destructive and non-destructive methods, Separations 11 (4) (2024) 122.
[2] L. Varanasi, et al., Transformations of dissolved organic matter induced by UV photolysis, hydroxyl radicals, chlorine radicals, and sulfate radicals in aqueous-phase UV-based advanced oxidation processes, Water Res. 135 (2018) 22–30.
[3] C. Ponraj, et al., Enhanced visible light photocatalytic activity of magnetic cobalt doped BiFeO3, Surfaces and Interfaces 31 (2022) 102050.
[4] Y. Wan, et al., Fabrication of graphene oxide enwrapped Z-scheme Ag2SO3/AgBr nanoparticles with enhanced visible-light photocatalysis, Appl. Surf. Sci. 396 (2017) 48–57.
[5] L. Bruner, J.J.Z.E.A.P.C. Kozak, Information on the photocatalysis I the light reaction in uranium salt plus oxalic acid mixtures, Z. Elektrochem. Angew. Phys. Chem. 17 (9) (1911) 354–360.
[6] N. Serpone, et al., On the genesis of heterogeneous photocatalysis: a brief historical perspective in the period 1910 to the mid-1980s, Photochem. Photobiol. Sci. 11 (7) (2012) 1121–1150.
[7] C.F. Goodeve, J.A.J.T.O.T.F.S. Kitchener, The mechanism of photosensitisation by solids, Trans. Faraday Soc. 34 (1938) 902–908.
[8] A.J.J.A.P.L. Nozik, Photochemical diodes, Appl. Phys. Lett. 30 (11) (1977) 567–569.
[9] R. Bickley, G. Munuera, F.J.J.O.C. Stone, Photoadsorption and photocatalysis at rutile surfaces: II. Photocatalytic oxidation of isopropanol, J. Catal. 31 (3) (1973) 398–407.
[10] S.N. Frank, A.J.J.J.O.T.A.C.S. Bard, Heterogeneous photocatalytic oxidation of cyanide ion in aqueous solutions at titanium dioxide powder, J. Am. Chem. Soc. 99 (1) (1977) 303–304.
[11] J.C. Colmenares, R.J.C.S.R. Luque, Heterogeneous photocatalytic nanomaterials: prospects and challenges in selective transformations of biomass-derived compounds, Chem. Soc. Rev. 43 (3) (2014) 765–778.
[12] C. Wu, et al., Nanoreactors for photocatalysis, Coord. Chem. Rev. 477 (2023) 214939.
[13] S. Fang, Y.H.J.C.S.R. Hu, Thermo-photo catalysis: a whole greater than the sum of its parts, Chem. Soc. Rev. 51 (9) (2022) 3609–3647.
[14] S. Guo, et al., Enhanced photocatalytic degradation of organic contaminants over CaFe2O4 under visible LED light irradiation mediated by peroxymonosulfate. Ournal of, Mater. Sci. Technol. 62 (2021) 34–43.
[15] A. Šutka, et al., Orthorhombic CaFe2O4: a promising p-type gas sensor, Sensors Actuators B 224 (2016) 260–265.
[16] Z. Zhou, et al., Electronic structure studies of the spinel CoFe2O4 by X-ray photoelectron spectroscopy, Appl. Surf. Sci. 254 (21) (2008) 6972–6975.
[17] S. Ali, et al., Charge transfer in TiO2-based photocatalysis: fundamental mechanisms to material strategies, Nanoscale 16 (9) (2024) 4352–4377.
[18] M.A.J.S.S.R. Henderson, A surface science perspective on TiO2 photocatalysis, Surf. Sci. Rep. 66 (6–7) (2011) 185–297.
[19] T.K. Tseng, et al., A review of photocatalysts prepared by sol-gel method for VOCs removal, Int. J. Mol. Sci. 11 (6) (2010) 2336–2361.
[20] M. Rauf, M. Meetani, S.J.D. Hisaindee, An overview on the photocatalytic degradation of azo dyes in the presence of TiO2 doped with selective transition metals, Desalination 276 (1–3) (2011) 13–27.
[21] A. Al-Kdasi, et al., Treatment of textile wastewater by advanced oxidation processes—a review, Global nest: the Int. 6 (3) (2004) 222–230.
[22] E.S. Elmolla, M.J.D. Chaudhuri, Comparison of different advanced oxidation processes for treatment of antibiotic aqueous solution, Desalination 256 (1–3) (2010) 43–47.
[23] A. Mota, et al., Advanced oxidation processes and their application in the petroleum industry: a review, Brazilian journal of petroleum and gas 2 (3) (2009).
[24] C. Ponraj, et al., A review on the visible light active BiFeO3 nanostructures as suitable photocatalyst in the degradation of different textile dyes, Environmental Nanotechnology, Monitoring & Management 7 (2017) 110–120.
[25] X. Li, J. Yu, M.J.C.S.R. Jaroniec, Hierarchical photocatalysts, Chem. Soc. Rev. 45 (9) (2016) 2603–2636.
[26] D. Sudha, P.J.C.E. Sivakumar, P.P. Intensification, Review on the photocatalytic activity of various composite catalysts, Chem. Eng. Process. 97 (2015) 112–133.
[27] S. Liang, et al., A novel Ag2O/g-C3N4 pn heterojunction photocatalysts with enhanced visible and near-infrared light activity, Sep. Purif. Technol. 210 (2019) 786–797.

[28] N. Wei, et al., Ag2O nanoparticle/TiO2 nanobelt heterostructures with remarkable photo-response and photocatalytic properties under UV, visible and near-infrared irradiation, Applied Catalysis B 198 (2016) 83–90.
[29] S. Hu, et al., Fe3+ doping promoted N2 photofixation ability of honeycombed graphitic carbon nitride: the experimental and density functional theory simulation analysis, Applied Catalysis B 201 (2017) 58–69.
[30] S. Hu, et al., Photocatalytic oxygen reduction to hydrogen peroxide over copper doped graphitic carbon nitride hollow microsphere: the effect of cu (I)-N active sites, Chem. Eng. J. 334 (2018) 410–418.
[31] E. Casbeer, et al., Synthesis and photocatalytic activity of ferrites under visible light: a review, Sep. Purif. Technol. 87 (2012) 1–14.
[32] L. Khanna, N.J.M.S.I.S.P. Verma, Synthesis, characterization and in vitro cytotoxicity study of calcium ferrite nanoparticles, Mater. Sci. Semicond. Process. 16 (6) (2013) 1842–1848.
[33] K.K. Kefeni, B.B.J.S.m., Mamba, and technologies, *photocatalytic application of spinel ferrite nanoparticles and nanocomposites in wastewater treatment*, Sustain. Mater. Technol. 23 (2020) e00140.
[34] D. Mehta, S. Mazumdar, S.J.J.O.W.P.E. Singh, Magnetic adsorbents for the treatment of water/wastewater—a review. Journal of water, Process. Eng. 7 (2015) 244–265.
[35] S. Rana, et al., On the suitability of nanocrystalline ferrites as a magnetic carrier for drug delivery: functionalization, conjugation and drug release kinetics, Acta Biomater. 3 (2) (2007) 233–242.
[36] A. Tomitaka, et al., Biocompatibility of various ferrite nanoparticles evaluated by in vitro cytotoxicity assays using HeLa cells, J. Magn. Magn. Mater. 321 (10) (2009) 1482–1484.
[37] H. Yin, H. Too, G.J.B. Chow, The effects of particle size and surface coating on the cytotoxicity of nickel ferrite, Biomaterials 26 (29) (2005) 5818–5826.
[38] H. Yang, et al., Water-soluble superparamagnetic manganese ferrite nanoparticles for magnetic resonance imaging, Biomaterials 31 (13) (2010) 3667–3673.
[39] K.C.-F. Leung, Y.-X.J.J.N.S. Wang, and technology, *Mn–Fe nanowires towards cell labeling and magnetic resonance imaging*, Nanowires science and technology (2010) 331–344.
[40] S. Rana, et al., Micelle based synthesis of cobalt ferrite nanoparticles and its characterization using Fourier transform infrared transmission spectrometry and Thermogravimetry, Mater. Chem. Phys. 124 (1) (2010) 264–269.
[41] S. Mohapatra, et al., Monodisperse mesoporous cobalt ferrite nanoparticles: synthesis and application in targeted delivery of antitumor drugs, J. Mater. Chem. A 21 (25) (2011) 9185–9193.
[42] G. Baldi, et al., Synthesis and coating of cobalt ferrite nanoparticles: a first step toward the obtainment of new magnetic nanocarriers, Langmuir 23 (7) (2007) 4026–4028.
[43] N. Sulaiman, et al., Superparamagnetic calcium ferrite nanoparticles synthesized using a simple sol-gel method for targeted drug delivery, Biomed. Mater. Eng. 26 (s1) (2015) S103–S110.
[44] R. Candeia, et al., Synthesis and characterization of spinel pigment CaFe2O4 obtained by the polymeric precursor method, Mater. Lett. 58 (5) (2004) 569–572.
[45] A. Samariya, et al., Size dependent structural and magnetic behaviour of CaFe2O4, Curr. Appl. Phys. 13 (5) (2013) 830–835.
[46] L. King. Calcium Ferrite as a Semiconductor for Microbially Assisted Photocatalytic Reduction of Carbon Dioxide, 2022, pp. 1–222.
[47] S. Chaveanghong, et al., Photocatalytic removal of 2-chlorophenol from water by using waste eggshell-derived calcium ferrite, RSC Adv. 13 (26) (2023) 17565–17574.
[48] H. Khan, et al., One-pot hydrothermal synthesis of a carbon quantum dot/CaFe 2 O 4 hybrid nanocomposite for carcinogenic Congo red dye degradation, RSC Adv. 13 (21) (2023) 14461–14471.
[49] H. Manjunatha, et al., Effectiveness of green-synthesized nickel-doped calcium ferrite nanoparticles in the X-ray/gamma radiation shielding applications, Prog. Nucl. Energy 170 (2024) 105137.
[50] R. Bharamagoudar, A. Patil, S.J.P.O.T.S.S. Mathad, Exploring Calcium–Zinc Ferrite Nanoparticles: Synthesis, Properties, and Applications, Phys. Solid State 66 (3) (2024) 71–76.
[51] V. Vidya, L.J.B.O.P. Revathy, and A. Sciences-Chemistry, Synthesis and characterization of calcium ferrite nanoparticles by solution combustion method, Bulletin of Pure & Applied Sciences-Chemistry 37 (1) (2018) 131–136.
[52] D. Hirabayashi, et al., Formation of brownmillerite type calcium ferrite (ca 2 Fe 2 O 5) and catalytic properties in propylene combustion, Catal. Lett. 110 (2006) 155–160.
[53] N.-O. Ikenaga, et al., H2S absorption behavior of calcium ferrite prepared in the presence of coal, Energy Fuel 19 (1) (2005) 170–179.
[54] H.C. Gomes, et al., Synthesis of calcium ferrite for energy storage applications, J. Alloys Compd. 921 (2022) 166026.
[55] Ismael, M.J.S.E.M. and S. cells, Ferrites as solar photocatalytic materials and their activities in solar energy conversion and environmental protection: a review, Sol. Energy Mater. Sol. Cells 219 (2021) 110786.
[56] R. Araujo, et al., CaFe 2 O 4 ferrite nanofibers via solution blow spinning (SBS), Cerâmica 66 (2020) 467–473.
[57] R.J. Fernandes, et al., Magnetic nanoparticles of zinc/calcium ferrite decorated with silver for photodegradation of dyes, Mater. Chem. Phys. 12 (21) (2019) 3582.
[58] B. Randhawa, K.J.B.O.M.S. Sweety, Calcium ferrite formation from the thermolysis of calcium tris (maleato) ferrate (III), Bull. Mater. Sci. 23 (2000) 305–307.
[59] A. El-Rafei, et al., Electrospun magnetically separable calcium ferrite nanofibers for photocatalytic water purification, J. Magn. Magn. Mater. 428 (2017) 92–98.
[60] S. Ansari, et al., Effect of manganese-doping on the chemical and optical properties of cobalt ferrite nanoparticles, Mater. Sci. Eng. B 300 (2024) 117134.
[61] A.C. Ulpe, T.J.C. Bredow, GW-BSE calculations of electronic band gap and optical Spectrum of ZnFe2O4: effect of cation distribution and spin configuration, ChemPhysChem 21 (6) (2020) 546–551.
[62] M.S. Amulya, et al., Sonochemical synthesis of NiFe2O4 nanoparticles: characterization and their photocatalytic and electrochemical applications, Applied Surface Science Advances 1 (2020) 100023.
[63] K.D. McDonald, B.M.J.I.C. Bartlett, Microwave synthesis of spinel MgFe2O4 nanoparticles and the effect of annealing on photocatalysis, Inorg. Chem. 60 (12) (2021) 8704–8709.
[64] T. Ajeesha, et al., Structural investigation of cu doped calcium ferrite (Ca1-xCuxFe2O4; x= 0, 0.2, 0.4, 0.6, 0.8, 1) nanomaterials prepared by co-precipitation method, J. Mater. Res. Technol. 18 (2022) 705–719.
[65] S.K. Pardeshi, R.Y.J.M.R.B. Pawar, Optimization of reaction conditions in selective oxidation of styrene over fine crystallite spinel-type CaFe2O4 complex oxide catalyst, Mater. Res. Bull. 45 (5) (2010) 609–615.
[66] J. Cao, et al., Fabrication of p-type CaFe2O4 nanofilms for photoelectrochemical hydrogen generation, Electrochem. Commun. 13 (3) (2011) 275–278.
[67] M.J. Pirouz, M.H. Beyki, F.J.F.C. Shemirani, Anhydride functionalised calcium ferrite nanoparticles: a new selective magnetic material for enrichment of lead ions from water and food samples, Food Chem. 170 (2015) 131–137.
[68] N. Sulaiman, et al., Synthesis and characterization of CaFe2O4 nanoparticles via co-precipitation and auto-combustion methods, Ceram. Int. 44 (1) (2018) 46–50.
[69] K. Petcharoen, A.J.M.S. Sirivat, E. B, Synthesis and characterization of magnetite nanoparticles via the chemical co-precipitation method, Mater. Sci. Eng. B 177 (5) (2012) 421–427.
[70] R.C.J.S.S.P. Pullar, Hexagonal ferrite fibres and nanofibres, Solid State Phenom. 241 (2016) 1–68.
[71] H. Liu, et al., Effect of temperature on the size of biosynthesized silver nanoparticle: deep insight into microscopic kinetics analysis, Arab. J. Chem. 13 (1) (2020) 1011–1019.
[72] S. Park, et al., Coprecipitation temperature effects of morphology-controlled nickel hexacyanoferrate on the electrochemical performance in aqueous sodium-ion batteries, ChemSusChem 14 (4) (2021) 1082–1093.
[73] H.S. Dehsari, et al., Effect of precursor concentration on size evolution of iron oxide nanoparticles, CrystEngComm 19 (44) (2017) 6694–6702.
[74] U. Lamdab, et al., Effect of a pH-controlled co-precipitation process on rhodamine B adsorption of MnFe 2 O 4 nanoparticles, RSC Adv. 8 (12) (2018) 6709–6718.
[75] L. Junliang, et al., One-step synthesis of barium hexaferrite nano-powders via microwave-assisted sol–gel auto-combustion, J. Eur. Ceram. Soc. 30 (4) (2010) 993–997.
[76] S. Bharadwaj, et al., A study of magnetic and dielectric properties for Iron ion variation in cobalt ferrite, In Spin 13 (2) (2023).
[77] G. Rajeswari, et al., An investigation of the correlation between the photovoltaic, magnetic and optical properties of CoCr2O4 due to the doping effect of rare-earth La3+ ions, Chemical Physics Impact 6 (2023) 100220.
[78] M. Sajjia, et al., Developments of cobalt ferrite nanoparticles prepared by the sol–gel process, Ceram. Int. 40 (1) (2014) 1147–1154.
[79] P. Jani, et al., Investigations of calcium ferrite nanoparticles synthesized by sol-gel auto combustion and solution mixture methods, Mater. Res. Innov. 26 (3) (2022) 189–195.
[80] M. Veith, M. Haas, V.J.C.O.M. Huch, Single source precursor approach for the sol− gel synthesis of nanocrystalline ZnFe2O4 and zinc− iron oxide composites, Chem. Mater. 17 (1) (2005) 95–101.
[81] C.J.I.F. Mamatha, Evaluation of structural properties of calcium hexaferrites on the basis of synthesis method. Ntegrated, Ferroelectrics 204 (1) (2020) 23–32.
[82] J. Ahmed, et al., Development of a microemulsion-based process for synthesis of cobalt (co) and cobalt oxide (Co3O4) nanoparticles from submicrometer rods of cobalt oxalate, ournal of colloid and interface science 321 (2) (2008) 434–441.
[83] G. Allaedini, S.M. Tasirin, P.J.I.N.L. Aminayi, Magnetic properties of cobalt ferrite synthesized by hydrothermal method. International, Nano Lett. 5 (2015) 183–186.
[84] G.J.J.O.M.C. Demazeau, Solvothermal processes: a route to the stabilization of new materials, J. Mater. Chem. A 9 (1) (1999) 15–18.
[85] Y. Xie, et al., A benzene-thermal synthetic route to nanocrystalline GaN, SCIENCE CHINA Chem. 272 (5270) (1996) 1926–1927.
[86] J. Huo, M.J.M.L. Wei, Characterization and magnetic properties of nanocrystalline nickel ferrite synthesized by hydrothermal method, Mater. Lett. 63 (13–14) (2009) 1183–1184.
[87] G. Allaedini, S.M. Tasirin, M.J.A.J.B.A.S. Pudukudy, Effect of PH on cobalt oxide nanoparticles prepared by co-precipitation method. Australian J. Basic, Appl. Sci. 8 (19) (2014) 243–247.
[88] D. Zhao, et al., Study on supercritical hydrothermal synthesis of CoFe2O4 nanoparticles, J. Supercrit. Fluids 42 (2) (2007) 226–233.
[89] G. Allaedini, A.J.J.O.N.I.C. Muhammad, Study of influential factors in synthesis and characterization of cobalt oxide nanoparticles. Journal of nanostructure, Chemistry 3 (2013) 1–16.
[90] L. Zhao, et al., Studies on the magnetism of cobalt ferrite nanocrystals synthesized by hydrothermal method, J. Solid State Chem. 181 (2) (2008) 245–252.
[91] J. Liu, et al., Crystallinity depends on choice of iron salt precursor in the continuous hydrothermal synthesis of Fe–co oxide nanoparticles, RSC Adv. 7 (59) (2017) 37436–37440.
[92] L.-Y. Meng, et al., The progress of microwave-assisted hydrothermal method in the synthesis of functional nanomaterials, Materials Today Chemistry 1 (2016) 63–83.

[93] S. Zhao, et al., Complex-surfactant-assisted hydrothermal synthesis of one-dimensional ZnO nanorods for high-performance ethanol gas sensor, Sensors Actuators B 286 (2019) 501–511.
[94] P.W. Dunne, et al., Continuous-flow hydrothermal synthesis for the production of inorganic nanomaterials, Phil. Trans. R. Soc. A 373 (2057) (2015) 20150015.
[95] Y. Zhou, et al., One-step hydrothermal synthesis of hierarchical ag/bi 2 WO 6 composites: in situ growth monitoring and photocatalytic activity studies, SCIENCE CHINA Chem. 56 (2013) 435–442.
[96] B. Abebe, et al., Summary on adsorption and photocatalysis for pollutant remediation: Mini review, J Encapsulation Adsorpt Sci 8 (4) (2018) 225–255.
[97] Z. Abdi, F. Maghazeii, D.J.J.O.C.S. Ghanbari, The effect of calcium perovskite and newly developed magnetic CaFe 2 O 4/CaTiO 3 perovskite nanocomposite on degradation of toxic dyes under UV–visible radiation, J. Clust. Sci. (2021) 1–13.
[98] M. Sundararajan, et al., Enhanced visible light photocatalytic degradation of rhodamine B using Ni1-xCaxFe2O4 (0≤ x≤ 0.5) nanoparticles: performance, kinetics and mechanism, Mater. Res. Bull. 154 (2022) 111911.
[99] D.S. Pereira, et al., Magnetoliposomes containing calcium ferrite nanoparticles for applications in breast cancer therapy, Pharmaceutics 11 (9) (2019) 477.
[100] E.P. Oaikhinan, R.D. Walker, B. Ralph, The Application of Scanning Electron Microscopy to the Identification of Calcium Ferrites in Iron Oxide Pellets / Rasterelektronenmikroskopische Identifizierung von Kalziumferriten in Eisenoxidpellets 23(9), 1986, pp. 441–449.
[101] Y. Wang, et al., Conductivity and magnetic properties of Zn0. 6Cu0. 4Cr0. 5La0. 04Fe1. 46O4/PPy composites prepared by in situ inverse microemulsion polymerization, React. Funct. Polym. 68 (11) (2008) 1587–1593.
[102] R.K. Selvan, et al., Combustion synthesis of CuFe2O4, Mater. Res. Bull. 38 (1) (2003) 41–54.
[103] S. Alhassan, et al., Preparation and optical properties of PVDF-CaFe2O4 polymer nanocomposite films, Polymers 15 (9) (2023) 2232.
[104] E.D. Jeong, et al., Physical and optical properties of nanocrystalline calcium ferrite synthesized by the polymerized complex method, J. Nanosci. Nanotechnol. 9 (6) (2009) 3568–3573.
[105] R. Dom, et al., Synthesis of solar active nanocrystalline ferrite, MFe2O4 (M: ca, Zn, mg) photocatalyst by microwave irradiation, Solid State Commun. 151 (6) (2011) 470–473.
[106] S. Pandey, et al., Fast and highly efficient removal of dye from aqueous solution using natural locust bean gum based hydrogels as adsorbent, Int. J. Biol. Macromol. 143 (2020) 60–75.
[107] S. Chakraborty, S. Chowdhury, P.D.J.C.P. Saha, Adsorption of crystal violet from aqueous solution onto NaOH-modified rice husk, Carbohydr. Polym. 86 (4) (2011) 1533–1541.
[108] I. Khan, et al., Nanoclay-mediated photocatalytic activity enhancement of copper oxide nanoparticles for enhanced methyl orange photodegradation, J. Mater. Sci. Mater. Electron. 31 (2020) 8971–8985.
[109] N. Tara, et al., Nano-engineered adsorbent for the removal of dyes from water: a review, Curr. Anal. Chem. 16 (1) (2020) 14–40.
[110] V. Chandanshive, et al., In situ textile wastewater treatment in high rate transpiration system furrows planted with aquatic macrophytes and floating phytobeds, Chemosphere 252 (2020) 126513.
[111] A.J.C.I. Shindy, Problems and solutions in colors, dyes and pigments chemistry: a review Chem, Int 3 (2) (2017) 97–105.
[112] B.J.J.N.M. Schwartz, What makes a chromophore? Nat. Mater. 7 (6) (2008) 427–428.
[113] J.-Y. Ni, et al., Construction of a ratiometric phosgene probe by chromophore formation from auxochrome, Talanta 236 (2022) 122826.
[114] M. Israr, et al., Sheet-on-sheet like calcium ferrite and graphene nanoplatelets nanocomposite: a multifunctional nanocomposite for high-performance supercapacitor and visible light driven photocatalysis, J. Solid State Chem. 293 (2021) 121646.
[115] H.M. Umair, et al., Ferroelectric, dielectric, magnetic and photocatalytic properties of Mn doped ca-hexaferrite prepared via microemulsion route, Mater. Chem. Phys. 307 (2023) 128152.
[116] M. Kamali, S. Sheibani, A.J.J.O.E.M. Ataie, Magnetic MgFe2O4–CaFe2O4 S-scheme photocatalyst prepared from recycling of electric arc furnace dust, J. Environ. Manag. 290 (2021) 112609.
[117] A.S. Priya, et al., Synthesis and structural, dielectric and photocatalytic properties of (Ti, La)-co-doped calcium ferrite ceramic powders, Arab. J. Sci. Eng. 47 (6) (2022) 7657–7667.
[118] H.M. Evans, W.J.S. Schulemann, The action of vital stains belonging to the benzidine group, SCIENCE CHINA Chem. 39 (1004) (1914) 443–454.
[119] C.J.B. Cooksey, Histochemistry, Quirks of dye nomenclature. 1. Evans blue, Biotech. Histochem. 89 (2) (2014) 111–113.
[120] L. Yao, et al., Evans blue dye: a revisit of its applications in biomedicine. Contrast media & molecular, Imaging 2018 (2018).
[121] J. Adarsha, et al., Green synthesis of nanostructured calcium ferrite particles and its application to photocatalytic degradation of Evans blue dye, Materials Today Chemistry 49 (2022) 777–788.
[122] A.A. Al-Gheethi, et al., Sustainable approaches for removing Rhodamine B dye using agricultural waste adsorbents: A review, Chemosphere 287 (2022) 132080.
[123] X. Chen, et al., Oxidation degradation of rhodamine B in aqueous by treatment system, International Journal of Photoenergy 2012 (2012).
[124] S. Merouani, et al., Influence of bicarbonate and carbonate ions on sonochemical degradation of rhodamine B in aqueous phase, J. Hazard. Mater. 175 (1–3) (2010) 593–599.
[125] M. Tuzen, A. Sarı, T.A.J.J.O.E.M. Saleh, Response surface optimization, kinetic and thermodynamic studies for effective removal of rhodamine B by magnetic AC/CeO2 nanocomposite, J. Environ. Manag. 206 (2018) 170–177.
[126] S. Kumari, et al., Nano ca–mg–Zn ferrites as tuneable photocatalyst for UV light-induced degradation of rhodamine B dye and antimicrobial behavior for water purification, Ceram. Int. 49 (8) (2023) 12469–12480.
[127] S. Sahu, et al., Fruit peel activated carbon—an efficient bioadsorbent for methylene blue dye: equilibrium, kinetic, and thermodynamic study, Environ. Sci. Pollut. Res. 27 (2020) 22579–22592.
[128] J.O. Amode, et al., Adsorption of methylene blue from aqueous solution using untreated and treated (Metroxylon spp.) waste adsorbent: equilibrium and kinetics studies. International journal of industrial, Chemistry 7 (2016) 333–345.
[129] Y. Kuang, X. Zhang, S.J.W. Zhou, Adsorption of methylene blue in water onto activated carbon by surfactant modification, Water Res. 12 (2) (2020) 587.
[130] S. Muzammal, et al., Polymer-supported nanomaterials for photodegradation: Unraveling the methylene blue menace, Energy Conversion and Management: X 22 (2024) 10054.
[131] R.S. Ballarin, et al., Methylene blue in sepsis and septic shock: a systematic review and meta-analysis, Front. Med. 11 (2024) 1366062.
[132] D. Dimbo, et al., Methylene blue adsorption from aqueous solution using activated carbon of spathodea campanulata. Methylene blue adsorption from aqueous solution using activated carbon of spathodea campanulata 21, 2024, p. 101910.
[133] H. Kahlert, G. Meyer, A.J.C. Albrecht, Colour maps of acid–base titrations with colour indicators: how to choose the appropriate indicator and how to estimate the systematic titration errors, ChemTexts 2 (2016) 1–28.
[134] A. Kassale, et al., Kinetics and modeling of the adsorption of methylene blue by the grafted cotton, J. Chem. Bio. Phy. Sci 5 (2) (2015) 1205–1216.
[135] J. Pomicpic, et al., Methylene blue removal by poly (acrylic acid)-grafted pineapple leaf fiber/polyester nonwoven fabric adsorbent and its comparison with removal by gamma or electron beam irradiation, Radiat. Phys. Chem. 172 (2020) 108737.
[136] P. Heidari, S.J.J.O.P. Masoudpanah, and C.O. Solids, Structural, magnetic and optical properties and photocatalytic activity of magnesium-calcium ferrite powders, J. Phys. Chem. Solids 148 (2021) 109681.
[137] M. Bagherzadeh, R.J.P., Kaveh, and photobiology, *new magnetically recyclable reduced graphene oxide rGO/MFe2O4 (M= ca, mg)/Ag3PO4 nanocomposites with remarkably enhanced visible-light photocatalytic activity and stability*, Photochem. Photobiol. 94 (6) (2018) 1210–1224.
[138] L. Guo, et al., Molten salt-assisted shape modification of CaFe2O4 nanorods for highly efficient photocatalytic degradation of methylene blue, Opt. Mater. 119 (2021) 111295.
[139] M. Bagherzadeh, R. Kaveh, H.J.J.O.M.C.A. Mahmoudi, Facile synthesis of a recyclable Pd-rGO/CNT/CaFe 2 O 4 nanocomposite with high multifunctional photocatalytic activity under visible light irradiation, J. Mater. Chem. A 7 (27) (2019) 16257–16266.
[140] E. Anthony, et al., Solar active heterojunction of p-CaFe2O4/n-ZnO for photoredox reactions, Environ. Technol. Innov. 20 (2020) 101060.
[141] Z. Yin, et al., Mechanism research of catalytic degradation of 1, 2-dichlorobenzene over highly efficient hollow calcium ferrite by in situ FTIR spectra, Materials Today Energy 26 (2022) 100996.
[142] M. Kaur, et al., Synthesis of CaFe2O4-NGO nanocomposite for effective removal of heavy metal ion and photocatalytic degradation of organic pollutants, Nanomaterials 11 (6) (2021) 1471.
[143] G.K. Kara, et al., A novel and green heterogeneous photocatalytic system (Ca0. 01Fe2. 99O4/CaTiO3 nanocomposite): protocol synthesis, characterization, and study of photo-decoloration activity, Mater. Chem. Phys. 259 (2021) 124062.
[144] S. Shenoy, et al., Simple tactic polycondensation synthesis of Z-scheme quasi-polymeric g-C3N4/CaFe2O4 composite for enhanced photocatalytic water depollution via pn heterojunction, Chem. Eng. J. 453 (2023) 139758.
[145] E.B. Simsek, Ö.J.P.T. Tuna, Building synergism through heterojunction of n-CaTiO3 with p-CaFe2O4 for upgraded photocatalytic degradation of pharmaceuticals, Powder Technol. 411 (2022) 117945.
[146] I. Bouatam, et al., Solar photodegradation of rose Bengal in water on the spinel CaFe2O4, Optik 266 (2022) 169635.
[147] Q. Huang, et al., Accelerated photodegradation of T-2 toxin over magnetic recyclable ZnO/CaFe2O4 nanocomposite with a pn based Z-scheme heterojunction architecture, Sep. Purif. Technol. 347 (2024) 127518.